END
DATE
FILMED
8-80
DTIC

1.0

1.1

1.25 1.4 1.6

2.8 2.5
3.2 2.2
3.6
4.0 2.0

1.8

MICROCOPY RESOLUTION TEST CHART
NATIONAL BUREAU OF STANDARDS-1963-A

ASL-CR-80-0008-3

LEVEL II ⑫

ON THE ANALYTICAL INVERSION OF LIDAR RETURNS FROM AN INHOMOGENEOUS ATMOSPHERE

APRIL 1980

Prepared by

JAMES D. KLETT

New Mexico State University
Physical Science Laboratory
Box 3-PSL
Las Cruces, New Mexico 88003

DTIC
SELECTED
JUN 2 5 1980
E

US Army Electronics Research and Development Command
ATMOSPHERIC SCIENCES LABORATORY
White Sands Missile Range, NM 88002

ADA085922

DDC FILE COPY

80 6 20 012

NOTICES

Disclaimers

REPORT DOCUMENTATION PAGE		READ INSTRUCTIONS BEFORE COMPLETING FORM
1. REPORT NUMBER ASL-CR-80-0008-3	2. GOVT ACCESSION NO. AD-A085 922	3. RECIPIENT'S CATALOG NUMBER
4. TITLE (and Subtitle) ON THE ANALYTICAL INVERSION OF LIDAR RETURNS FROM AN INHOMOGENEOUS ATMOSPHERE		5. TYPE OF REPORT & PERIOD COVERED Technical Report
		6. PERFORMING ORG. REPORT NUMBER
7. AUTHOR(s) James D. Klett		8. CONTRACT OR GRANT NUMBER(s) DAAD07-79-C-0008
9. PERFORMING ORGANIZATION NAME AND ADDRESS New Mexico State University Physical Science Laboratory Las Cruces, New Mexico 88003		10. PROGRAM ELEMENT, PROJECT, TASK AREA & WORK UNIT NUMBERS 1L162111AH71-23
11. CONTROLLING OFFICE NAME AND ADDRESS US Army Electronics Research and Development Command Adelphi, MD 20783		12. REPORT DATE April 1980
		13. NUMBER OF PAGES 50
14. MONITORING AGENCY NAME & ADDRESS(if different from Controlling Office) Atmospheric Sciences Laboratory White Sands Missile Range, NM 88002		15. SECURITY CLASS. (of this report) UNCLASSIFIED
		15a. DECLASSIFICATION/DOWNGRADING SCHEDULE

16. DISTRIBUTION STATEMENT (of this Report)

Approved for public release; distribution unlimited

17. DISTRIBUTION STATEMENT (of the abstract entered in Block 20, if different from Report)

18. SUPPLEMENTARY NOTES

Contract Monitor: Jagir Randhawa

19. KEY WORDS (Continue on reverse side if necessary and identify by block number)

Lidar
Inhomogeneous
Atmosphere

Attenuation and backscatter
Coefficients
Inversion method

20. ABSTRACT (Continue on reverse side if necessary and identify by block number)

A new analytical method is presented for extracting attenuation and backscatter coefficients in an inhomogeneous atmosphere from the return signal of a monostatic, single wavelength lidar system. The inversion method can be applied using only information contained in the signal itself and, in sharp contrast to a well known related analytical inversion method, it is relatively tolerant of various characteristic errors and uncertainties. Inversion examples for a variety of conditions are presented and discussed.

DD FORM 1473 EDITION OF 1 NOV 65 IS OBSOLETE

1

CONTENTS

Accession For

NTIS GRA&I	✓
DDC TAB	☐
Unannounced	
Justification	

By_____

Distribution/_____

Availability Codes

| Dist | Avail and/or special |
| A | |

LIST OF FIGURES

I.   Introduction

An early and continuing goal of lidar research has been to devise an inversion method whereby profiles of optical parameters such as attenuation and backscatter coefficients in an inhomogenous atmosphere can be quickly and accurately deduced from the return signal of a monostatic, single wavelength lidar system. This is a problem area where, as expressed by Collis and Russell in an excellent review article "... the early promise of lidar has not yet been fulfilled" [1]. Some of the difficulties encountered along the way have been due to limitations in lidar performance and associated data processing technology, while others follow from theoretical requirements and constraints peculiar to the inversion process. This article addresses some aspects of the latter category of problems, and presents in particular a simple inversion method based on a new form of a well-known analytical solution.

II.   Review of the "Slope" and "Solution" Methods of Inversion

For a monostatic, single wavelength, pulsed lidar, the assumed basic governing form is the single-scattering lidar equation:

$$P(r) = Po \frac{c\tau}{2} A \frac{\beta(r)}{r^2} \exp[-2\int_{o}^{r}\sigma(r')dr'] \tag{1}$$

In this equation $P(r)$ is the instantaneous received power at time t, Po the transmitted power at time t_o, c the velocity of light, τ the pulse duration, A the effective system receiver area, $r(=c(t-t_o)/2)$ is the range, and $\beta(r)$ and $\sigma(r)$ are respectively the volume backscatter

5

and attenuation coefficients of the atmosphere. A more convenient signal variable is the logarithmic, range-adjusted power, defined as

$$S(r) = \ln[r^2 P(r)] \qquad (2)$$

In terms of $S = S(r)$ and $So = S(r_o)$, where r_o is a given constant reference range, Eq. (1) may be expressed in a system-independent form:

$$S - So = \ln \frac{\beta}{\beta_o} - 2 \int_{r_o}^{r} \sigma dr', \qquad (3)$$

where $\beta_o = \beta(r_o)$.

The differential equation corresponding to Eq. (3) is

$$\frac{dS}{dr} = \frac{1}{\beta} \frac{d\beta}{dr} - 2\sigma, \qquad (4)$$

a solution which evidently requires knowing or assuming a relationship between β and σ whenever $d\beta/dr \neq 0$. On the other hand, if the atmosphere is homogeneous so that $d\beta/dr = 0$, the attenuation coefficient can be expressed directly in terms of the signal slope:

$$\sigma_{hom.} = -\frac{1}{2} \frac{dS}{dr} \qquad (5)$$

This is the basis of the slope method of inversion [2,3], in which typically the slope of the least squares straight line fit to the curve $S = S(r)$ is used as the best estimate of dS/dr over any interval where S itself appears to be nearly a straight line.

6

Going a step further, it has often been assumed that since the atmosphere is more likely to be homogeneous over small rather than large intervals, by applying the slope method to a succession of small intervals a reasonable first approximation to $\sigma = \sigma(r)$ in a notably inhomogenous atmosphere may also be achieved. From Eq. (4) it is clear this amounts to a conjecture that generally $\beta^{-1}\left|d\beta/dr\right| << 2\sigma$, at least over most of the S curve. Unfortunately, assumptions like this appear not to be well justified for many situations of interest, e.g., under conditions of dense cloud, fog, smoke, and dust. Even under the relatively stable conditions prevailing in fogs, significant local heterogeneities occur. For example, the spatial variation of fog drop concentrations is often quite large, ranging up to two orders of magnitude for certain size categories [4,5]. Such micro-structure variation along the lidar beam path could easily lead to relatively large fluctuations in $d\beta/dr$, hence invalidating local application of the slope method. The same criticism applies to the so called "ratio" or "slice" method of inversion [6,7], which is merely an extremely close variant of the slope method as applied to successive range intervals. (Additional discussion on the merits of the slope and ratio methods is available through the recent articles of Kohl [8, 9] and Brown [10]. Also, a theoretical example which illustrates the inadequacy of the slope method for a case of high visibility is given below in Section V.)

Several observational and theoretical studies have been published which show that under a wide range of realistic circumstances β and σ can in fact be related approximately according to a power law of the form

$$\beta = \text{const. } \sigma^k, \tag{6}$$

7

where k depends on the lidar wavelength and various properties of the obscuring aerosol. Reported values of the exponent are generally on the interval $0.67 \leq k \leq 1.0$ [11-15]. If such a relationship is assumed, Eq. (4) becomes

$$\frac{dS}{dr} = \frac{k}{\sigma} \frac{d\sigma}{dr} - 2\sigma \qquad (7)$$

Although the above ordinary differential equation is nonlinear, it nevertheless has an elementary structure, namely that of the homogeneous Ricatti equation [16]. For a very long time (at least over 100 years) it has been known that equations of this type may be transformed to a first order linear form by introducing a new unknown equal to the reciprocal of the original. The general solution can therefore be easily written down as

$$\sigma^{-1} = \exp\left(-\int^r \frac{1}{k} \frac{dS}{dr'} \, dr'\right)\left[C - 2\int^r \frac{\exp}{k}\left(-\int^{r'} \frac{1}{k} \frac{dS}{dr''} \, dr''\right) dr'\right], \qquad (8)$$

where C is the integration constant. If k is regarded as constant, which appears not to be unduly restrictive and shall be assumed here for brevity, a well known form of the solution may be obtained:

$$\sigma = \frac{\exp[(S - S_0)/k]}{\left(\sigma_0^{-1} - \frac{2}{k} \int_{r_0}^{r} \exp[(S - S_0)/k] dr'\right)}, \qquad (9)$$

where $\sigma_0 = \sigma(r_0)$. The first appearance of Eq. (9) or its equivalent in the literature on remote sensing was apparently in 1954 in the context of rain intensity measurements by radar at attenuating wavelengths [17].

It has since re-emerged in several articles on the interpretation
of lidar measurements [3, 18-20].

In spite of the evident theoretical superiority of Eq. (9)
over the slope method (which corresponds to setting $k = 0$ in
Eq. (7)), it is the latter method which is most often used. This is
because Eq. (9) has a tendency to produce at best marginal results,
and in practice has likely been more a source of frustration than a
useful tool for analyzing radar or lidar returns. For example, in
their 1954 article referred to above, Hitschfeld and Bordan [17]
concluded it was probably not possible to calibrate a radar set
accurately enough to make use of the solution, and that rainfall
measurements made without correcting for attenuation via the solu-
tion are in many cases more accurate than the corrected values.
Worse yet, others have noted the solution may lead to "... absurdly
large, infinite, or negative values..." [18] and "... physically
meaningless..." [21] results. Others have avoided such behavior
only by using unrealistically large values of k [3].

There is surprisingly little comment in the literature on the
reasons for the failure of Eq. (9). It seems only to be somewhat
vaguely attributed to the omission of multiple scattering effects
[1, 7]. However, since the slope method suffers from the same
deficiency, but with apparently much less drastic consequences,
this explanation is not very convincing.

Unfortunately, only a few relevant studies on the possible importance of multiple scattering are available. In one of these, Viezee et. al. [7] compared lidar and transmissometer measurements in dense fog and found an apparent 10 to 45% overprediction of lidar-derived visibilities using the slope method. They conjectured this discrepancy was due to the influence of forward and multiple scattering and proposed an empirical correction to the slope method for use under turbid atmosphere conditions. On the other hand, they also noted that available theoretical descriptions of multiple scattering [22-24] could not account for the observed discrepancies in the lidar and transmissometer data. A later Monte Carlo simulation of second and third order multiple scattering in dense, homogeneous fog led to the conclusion that multiply scattered radiation will cause the slope method to be in error by less than about 10% for visibilites of the order of 100m [25].

From these studies it appears unlikely that even for a dense dispersion the contribution of multiply scattered radiation could make a crucial difference in the applicability of Eqs. (1) or (9). Therefore, although it would certainly be desirable to replace Eq. (1) with a new governing form containing higher scattering approximations (perhaps, for example, along the lines recently outlined by Samokhvalov [26]), there seems at present no justification for regarding the inclusion of multiply scattered radiation effects as the sine qua non for the inversion of lidar signals from a markedly inhomogenous atmosphere. (In this regard it should be recalled also that the traditional description of Eq. (1) as the

single scattering lidar equation is a misnomer, since Eq. (1) incorporates the assumption that backscattered photons are also attenuated; hence it does include some multiple scattering effects.)

From a purely mathematical point of view, it is easy to see the problem with Eq. (9): Since on average the signal decays with range beyond r_o due to attenuation, σ is determined as the ratio of two numbers which each become progressively smaller with increasing r; furthermore, the denominator, which must approach zero at nearly the same rate as the numerator, is expressed as the difference between two relatively large numbers. Such structure produces a strong tendency for instability and suggests that unattainable accuracy in the determination of σ_o may often be requisite for avoiding a singularity, even for signals which are free of noise.

The above description may be illustrated quantitatively by considering the growth of a small perturbation in σ due to an error δo in the determination of σ_o. For the same signal let σ be the solution corresponding to σ_o, and $\sigma' = \sigma + \delta$ be the solution corresponding to $\sigma'_o = \sigma_o + \delta_o$. Then from the integrated form of Eq. (7) it follows that

$$S - So = k \ln \frac{\sigma}{\sigma_o} - 2 \int_{r_o}^{r} \sigma dr \qquad (10)$$

$$= k \ln \frac{\sigma'}{\sigma'_o} - 2 \int_{r_o}^{r} \sigma' dr,$$

11

which implies

$$(1 + \delta/\sigma) = (1 + \delta_0/\sigma_0) \exp \left(\frac{2}{k} \int_{r_0}^{r} \delta dr\right) \tag{11}$$

For simplicity consider a homogeneous atmosphere with $\sigma = \sigma_0$. Then by differentiating Eq. (11) one obtains

$$\frac{d\zeta}{dr} = \frac{2}{k} \sigma_0 \zeta(\zeta - 1),$$

where $\zeta = (1 + \delta/\sigma_0)$. This is a homogeneous Ricatti equation, like Eq. (7), with a solution given by

$$\left(1 + \frac{\delta}{\sigma_0}\right)^{-1} = 1 - \frac{\delta_0}{\sigma_0} \left(1 + \frac{\delta_0}{\sigma_0}\right)^{-1} \exp\left[\frac{2\sigma_0(r - r_0)}{k}\right] \tag{12}$$

From this expression it can be seen that an underestimate of σ ($\delta_0 < 0$) leads to $\delta \to -\sigma_0$ (i.e., $\sigma \to 0$) as $r \to \infty$. On the other hand, if σ_0 is overestimated ($\delta_0 > 0$), then $\sigma \to \infty$ within a finite distance given by

$$\Delta r = \frac{k}{2\sigma_0} \ln \left(1 + \frac{\sigma_0}{\delta_0}\right) \tag{13}$$

For example, if $\sigma_0 = 10$ km^{-1}, $k = 1$, and $\delta_0/\sigma_0 = 10^{-2}$, then the solution has a singularity within about the next 231 meters; also, for $r > r_0 + \Delta r$ the solution is negative. This example is also shown in Figure 1, where the unit of length for range plotted along the abscissa has been set equal to 0.010 km (10m), and attenuation per km is plotted along the ordinate. (This same choice f units is

12

used for all the theoretical curves of $\sigma = \sigma(r)$ given in this paper. Corresponding curves of $S - S_0$ vs. r use the same range scale; $S - S_0$ is of course dimensionless.) The tendencies shown in Figure 1 are accentuated by larger σ_0/k (lower visibilities) and larger δ_0/σ_0 (poorer estimates of σ_0).

Finally, substitution of Eq. (12) back into Eq. (10) reproduces the original signal, $S - S_0 = -2\sigma_0(r-r_0)$, independently of the value of δ_0. Therefore, two main points should be emphasized regarding these results: 1) Eq. (9) is - to loosely paraphrase a terminology used in analogous, though generally more complicated circumstances - "ill constructed", in that small differences in the choice of boundary value σ_0 provide no assurance that the corresponding solutions will remain close for $r > r_0$. 2) Closeness of the $S(\sigma)$ curve, reconstructed from the solution for σ, to the original S curve is insufficient to guarantee the reasonableness of the solution. (Such closeness has been used in the past as a test of validity of the solution [3].) Because of this behavior one would expect, and experience has shown, that Eq. (9) by itself is of very little practical value.

III. A New Solution Form

It is fortunately quite easy to select a different and more appropriate solution form than Eq. (9). One merely has to evaluate the integration constant C in Eq. (8) in terms of a reference range r_m such that the solution is generated for $r \leq r_m$, rather than for $r \geq r_0$ as before. For constant k the result is

13

$$\sigma(r) = \frac{\exp[(S - S_m)/k]}{\left(\sigma_m^{-1} + \frac{2}{k} \int\limits_{r}^{r_m} \exp\,[(S - S_m)/k]\,dr'\right)}, \qquad (14)$$

where $S_m = S(r_m)$ and $\sigma_m = \sigma(r_m)$. This seemingly innocuous change from Eq. (9) makes a very significant difference in the behavior of the solution. As r decreases from r_m, σ is now determined as the ratio of two numbers which each become progressively larger, so that stability and accuracy are easy to maintain. The form of the denominator also indicates that the dependence of the solution on σ_m decreases with decreasing r.

The contrasting behavior of Eqs. (9) and (14) is illustrated in Figure 2. (In this and several subsequent figures, displays are given of various "inversions" (solutions of Eqs. (9) and (14)) of signals generated by Eq. (10) in response to specified σ distributions. The value k = 1 was used in the computations, except where otherwise indicated. (The choice of k is of course not important so long as the same value is used for generating the signal as for inverting it.)) Figure 2(a) shows the signal response to the platform distribution of σ given in Figure 2(b). Also in Figure 2(b) are shown the signal inversions from Eq. (9) for boundary values which are in error by ±1%. Figure 2(c) displays the corresponding inversions from Eq. (14) for boundary values which are in error by ±50%. The relatively small effect of a poor boundary value estimate on Eq. (14) is obvious.

14

Analogous differences in the capacities of the inversions to survive simulated signal noise are shown in Figure 3. Figure 3(a) displays three superposed signals, the first being due to a constant attenuation of 10 km^{-1}, and the others being like the first except for ±10% "blips" on the interval (30,32). Figures 3(b) and 3(c) give the respective corresponding signal inversions from Eqs. (9) and (14), wherein the correct boundary value has been used for all solutions. It can be seen that the solution of Eq. (9) is obliterated for ranges beyond the point noise is encountered, whereas Eq. (14) displays a strong tendency to recover from signal errors.

The effect of an incorrect value of k is illustrated in Figure 4, where again the computations are based on the platform-shaped distribution of attenuation shown in the prior figures, and k = 1 was used to generate the signal (shown in Figure 2(a)). In Figure 4(a) it can be seen that as soon as the signal slope varies, so that the value of k enters into the calculations, the inversion based on Eq. (9) fails. The much weaker impact on Eq. (14), illustrated in Figure 4(b), indicates great accuracy in the determination of k is not required.

In summary, these examples show that Eq. (14) is relatively insensitive to the kinds of errors that are likely to effect the inversion of real signals. Especially encouraging is the tendency of Eq. (14) to approach the correct solution curve in spite of a poor estimate of the boundary value, σ_m. This raises the hope that difficult, accurate "lidar calibrations" or independent measurements of some optical parameter at a reference point, or through a given

15

layer, may not be necessary, at least for the majority of applications. In the next section, the question of how to make a reasonable, self-contained estimate of σ_m from the signal alone is considered.

IV. Estimation of σ_m; Generalization of the Slope Method

It would appear to be a relatively straightforward matter to obtain a good estimate for σ_m, in view of the following circumstance: Assuming the validity of the lidar equation, Eq. (1), and the constitutive relation, Eq. (6), and assuming also that σ varies linearly over a specified interval (r_a, r_b), then it is possible to express σ solely in terms of the signal over the interval. This follows directly from integration of Eqs. (9) and (14) over (r_a, r_b), with $S_o \rightarrow S_a = S(r_a)$ and $S_m \rightarrow S_b = S(r_b)$:

$$\int_{r_a}^{r_b} \sigma dr = \frac{-k}{2} \ln \left[1 - \frac{2\sigma_a}{k} \int_{r_a}^{r_b} \exp[(S - S_a)/k]dr' \right] , \qquad (15)$$

$$\int_{r_a}^{r_b} \sigma dr = \frac{k}{2} \ln \left[1 + \frac{2\sigma_b}{k} \int_{r_a}^{r_b} \exp[(S - S_b)/k]dr' \right] , \qquad (16)$$

where $\sigma_a = \sigma(r_a)$ and $\sigma_b = \sigma(r_b)$. Because of the assumed linear variation of σ over (r_a, r_b), the average value of σ on the interval is just $\bar{\sigma} = (\sigma_a + \sigma_b)/2$. Therefore, Eqs. (15) and (16) may be combined to predict the values of $\bar{\sigma}$, σ_a, or σ_b. For example, $\bar{\sigma}$ is obtained from the solution of the equation

$$\Omega = \frac{(1 - \exp(-\Omega))}{2I_{ab}} + \frac{(\exp(\Omega) - 1)}{2I_{ba}} , \qquad (17)$$

16

where

$$\Omega = \frac{2\bar{\sigma}(r_b - r_a)}{k},$$ (18)

$$I_{ab} = (r_b - r_a)^{-1} \int_{r_a}^{r_b} \exp[(S - S_a)/k]dr',$$ (19)

and

$$I_{ba} = (r_b - r_a)^{-1} \int_{r_a}^{r_b} \exp[(S - S_b)/k]dr' = I_{ab} \exp[(S_a - S_b)/k]$$ (20)

Since the assumption that σ is linear will become better with decreasing interval size, the application of Eqs. (17) - (20) over a succession of small intervals would appear in principle to constitute an inversion of the lidar signal which does not require any information beyond that contained in the signal itself. In practice however, the local structure of the signal is not known well enough to ensure the success of such a method. This can be seen by considering the form of the solution to Eqs. (17) - (20) for the case that $\Omega \ll 1$, i.e., for intervals $\Delta r \ll k/2\bar{\sigma}$. By expansion of I_{ab} and I_{ba} to include terms proportional to Δr^2, the solution for $\bar{\sigma}$ is found to be

$$\bar{\sigma} = \frac{-3(S'_a + S'_b)}{16}\left\{1 + \left[1 - \frac{16}{9(S'_a + S'_b)^2}\left(S'^2_a + S'^2_b + k(S''_a + S''_b)\right)\right]^{\frac{1}{2}}\right\},$$ (21)

where $S'_a = (dS/dr)r_a$, $S'_b = (dS/dr)r_b$, $S''_a = (d^2S/dr^2)r_a$, and $S''_b = (d^2S/dr^2)r_b$. This generalization of the slope method result, Eq. (5), is certainly more rigorous in its account of the local geometry of the signal. Unfortunately however, the new terms

17

representing signal curvature are extremely difficult to estimate, so that point-by-point application of Eqs. (17) - (20) or (21) can generally be expected to provide little real improvement over the slope method.

An example of the point-by-point use of Eq. (21) is shown in Figure 5(b). For the platform distribution used to generate the lidar signal, the curvature is zero everywhere except at the points where the slope changes abruptly, and at these points it becomes infinite. The obvious departures of the inversion curve shape from the platform distribution are due to the effective numerical diffusion of the input delta function distribution of curvature. Thus even for this theoretical example wherein the lidar signal appears quite smooth and is known to a high degree of accuracy, significant errors occur in the estimation of signal curvature.

However, in defense of Eq. (21) it is also worth noting that its point-by-point application, in conjunction with an algorithm to smooth the signal, will generally permit a good recovery of the broad features of an attenuation distribution. An example to this effect is given in Figure 5(c). For the inversion shown the signal in Figure 5(a) was smoothed 15 times (according to the simple scheme that $S_i \rightarrow (S_{i+1} + S_i + S_{i-1})/3$), subject of course to the constraint of fixed curve end points. In general it appears adequate to smooth the signal until $|S''/S'^2| \lesssim 10^{-1}$. Finally, the inversion displayed in Figure 5(c) also produces nearly the same $\bar{\sigma}$ for the entire range as does the input distribution. This happens because $\bar{\sigma}$ depends only on $S_b - S_a$ whenever $\sigma_a = \sigma_b$, as is evident from Eq. (10). Thus for

18

situations in which the endpoint values of attenuation are known to be approximately equal (e.g., a localized obscurant in otherwise clear air), the use of Eq. (21) with signal smoothing will not result in a significant error in the estimate of total optical depth,

$$\int_{r_a}^{r_b} \sigma dr = \bar{\sigma}(r_b - r_a).$$

Although Eqs. (17) - (20) or Eq. (21) can be used to provide estimates of σ_m, the above discussion suggests there may on occasion be instability problems for signals with "rough" structure. Greater stability may of course be achieved by choosing a larger integration interval, but offsetting this is the decreasing likelihood that σ remains linear over larger intervals. An alternative which is not as impaired by the attempt to incorporate more signal information over a larger interval is the following: From Eq. (16) one can write

$$\int_{r_a}^{r_b} \sigma dr = \int_{r_a}^{r_c} \sigma dr - \int_{r_b}^{r_c} \sigma dr = \frac{k}{2} \ln \left[\frac{\dfrac{k \exp(S_c/k)}{2\sigma_c} + \displaystyle\int_{r_a}^{r_c} \exp(S/k)dr'}{\dfrac{k \exp(S_c/k)}{2\sigma_c} + \displaystyle\int_{r_b}^{r_c} \exp(S/k)dr'} \right] \quad (22)$$

where $r_c > r_b > r_a$. For $r_c \gg r_a$, r_b the right hand side of this expression will be only weakly dependent on σ_c. Imagine now a hypothetical linear extension of the signal curve beyond r_m with a slope $-A$ equal, for example, to the mean slope of the curve over the range of interest for $r_0 \leq r \leq r_m$; i.e., let $r_c > r_m > r_b$ and set $S = S_m - A(r - r_m)$ for $r_m \leq r < r_c$. Then

$$\int_{r_a}^{r_c} \exp \frac{S}{k}\, dr' = \int_{r_a}^{r_m} \exp\left(\frac{S}{k}\right) dr' + \frac{k}{A} \exp\left(\frac{S_m}{k}\right) \left[1 - \exp\left(\frac{-A(r_c - r_m)}{k}\right)\right],$$

so that for $r_c \gg r_m$ Eq. (22) becomes

$$\int_{r_a}^{r_b} \sigma dr \cong \frac{k}{2} \ln\left[\frac{\frac{k}{A} + \int_{r_a}^{r_m} \exp[(S - S_m)/k]dr'}{\frac{k}{A} + \int_{r_b}^{r_m} \exp[(S - S_m)/k]dr'}\right] \tag{23}$$

By substituting this result into Eq. (16), a corresponding estimate of σ_b may be obtained.

Trial applications of Eq. (23) have shown that fairly good results may usually be achieved by setting $A = (S_o - S_m)/(r_m - r_o)$ and choosing $r_b - r_o$ to be as large as within a few percent of $r_m - r_o$. The interval (r_a, r_b) may, if desired, be taken as small as the basic increment between data points. One may then use σ_b so obtained along with Eq. (14) (letting $r_m \rightarrow r_b$, etc.) to generate the solution over (r_o, r_b). Alternatively, one may further approximate $\sigma_m \cong \sigma_b$ and generate the solution over (r_o, r_m).

V.   Inversion Examples and Discussion

Some examples of inversions generated according to the procedure described above are shown in Figures 6 - 8. In terms of the range variable $x = r/10$ (r in meters) plotted along the abscissa, the inversions shown were obtained from Eqs. (14), (16), and (23) using

$x_a = 90$, $x_b = 91$, and $x_m = 100$. (However, it should be noted that these choices are not special ones required to produce the degree of accuracy displayed in the figures; other similar choices produce similar results, and indeed such relative insensitivity to the choices of x_a and x_b provides a qualitative indication that the inversions are not seriously in error.) The overall accuracy of the inversions can be seen to be quite good. For the distribution shown in Figure 6(b) the average value of the input attenuation over the entire range is $\bar{\sigma}_{in} = 32.5$ km^{-1}, whereas the inversion value is $\bar{\sigma}_{out} = 32.8$ km^{-1}. Also shown in Figure 6(b) is an inversion based on the smoothed signal in Figure 6(a) (smoothed 10 times in accordance with the prescription given earlier); for it the average attenuation is $\bar{\sigma}_{out} = 33.2$ km^{-1}. For the distribution shown in Figure 7(b) the corresponding values are $\bar{\sigma}_{in} = 38.5$ km^{-1} and $\bar{\sigma}_{out} = 38.8$ km^{-1}, the difference in this case being due almost entirely to a slight inversion misrepresentation at the bottoms of the "troughs".

It is clear from Figures 6 and 7 that the inversion procedure can recover considerable detail from the signal. In this regard it is also noteworthy that special numerical processing is not necessary to obtain good resolution. The computations used to generate the figures involved only one slightly nonstandard procedure, namely that of fitting the signal curve point-by-point with a composite cubic spline [26], in order to provide greater accuracy in the interpolation of the signal between base points. The subsequent numerical integrations were all carried out via Simpson's rule in single precision. However, nearly equivalent accuracy can be

obtained by using just single precision, point-by-point trapezoidal rule integration without interpolation. This simpler approach should be more than adequate in applications in view of the many other relevant theoretical and experimental limitations.

Examples of inversions under high visibility conditions are shown in Figure 8. For this case with $\sigma \cong 10^{-1}$ km^{-1}, the structure visible in the signal is due to the predominance of the first term on the right hand side of Eq. (7) or (10); i.e., the signal variation is caused mainly by changes in the fractional gradient of attenuation, rather than by changes in attenuation magnitude. Consequently, the slope method of inversion applied to small intervals gives erroneous results for a situation ironically representative of those for which it is generally assumed most applicable. The failure of the point-by-point application of the slope method is shown vividly by the dashed curve in Figure 8(a). Even if one were to ignore signal curve portions where negative values of σ are predicted (a strategy used in the past by slope method practitioners), the predicted positive excursions in σ are grossly overstated. (On the other hand, it should also be noted that the slope method applied to the entire range interval provides an excellent estimate for $\bar{\sigma}$.) The fine structure of the input and inversion distributions is revealed in the expanded ordinate scale of Figure 8(b). The corresponding values of average attenuation are $\bar{\sigma}_{in} = 0.101$ km^{-1} and $\bar{\sigma}_{out} = 0.102$ km^{-1}. An interesting new feature shown here is the tendency of the misfit at the boundary point r_m to carry on through the length of the inversion. There is insufficient optical depth for the inversion method to rapidly approach the true solution curve.

22

Figures 9 and 10 illustrate situations where an additional small computational step can improve the accuracy of the inversion. If σ increases or decreases significantly over the range (r_o, r_m), then the use of Eq. (23) as described earlier biases the estimate of σ_m too much toward the value of $\bar{\sigma}$ over (r_o, r_m). Thus in Figure 9(b) σ_m is too small, whereas in Figure 10(b) it is too large. In such situations where the inversion reveals a fairly systematic trend in σ (or if such behavior is known independently, or can, e.g., be discerned directly by simple inspection of the signal), a better estimate of σ_m can be obtained by iterating Eq. (23) with A replaced by twice the current iterative value of σ_m (cf. Eq. (5)). This gives greater weight to the signal information available near r_m. An indication of the improvement this strategy can bring about is illustrated in Figures 9(b) and 10(b). A simpler alternative which is appropriate when it is known that σ is in a separate regime on some interval (r_a, r_m) near r_m (e.g., clear air on the far side of a smoke cloud, or clear air above an inversion) is simply to set $A = (S_a - S_m)/(r_m - r_a)$ in Eq. (23).

As a final example, inversions of a real lidar return from fog are shown in Figure 11. The laser used emitted pulses averaging 10 millijoules in 6 nanoseconds at 1.06 μm, and a 20 megahertz sampling rate transient recorder was used to produce sample points spaced 7.5 m apart over the lidar return [27]. The initial increase in the lidar signal shown in Figure 11(a) is due to increasing σ, and is not caused by incomplete overlap of the transmitter and receiver fields of view. The inversions are based on Eqs. (14), (16), and (23), with $A = (S_{15} - S_{30})/(r_{30} - r_{15})$. In Figure 11(b) are shown

23

the results for k = 1.0 and 0.67; the former value is probably better for fog, but in any case the inversions, as demonstrated earlier, do not depend strongly on the choice of k. For either value of k the average attenuation is $\bar{\sigma} = 13.0 \text{ km}^{-1}$. This result can be compared to the visibility as measured by a transmissometer during the same experiment. The transmissometer visibility $\bar{v}$ (km), based on a constrast threshold of 0.05 so that $\bar{v} = 3.0/\bar{\sigma}$, is 0.20 km [27]. The corresponding value from the lidar inversion is $\bar{v} = 0.23$ km. The extent of agreement is as good as could be expected, given just the uncertainties associated with the experimental data.

REFERENCES

1. R. T. H. Collis and P. B. Russell, in Laser Monitoring of the Atmosphere, E. D. Hinkley, Ed. (Springer, New York, 1976), p. 117.

2. R. T. H. Collis, Quart. J. Roy. Meteorol. Soc. 92, 220 (1966).

3. W. Viezee, E. E. Uthe, and R. T. H. Collis, J. Appl. Meteorol. 8, 274 (1969).

4. H. R. Pruppacher and J. D. Klett, Microphysics of Clouds and Precipitation (Reidel, Dordrecht, Holland, 1978), pp. 20-21.

5. T. Okita, J. Meteorol. Soc. Japan, 40, 39 (1962).

6. R. T. Brown, Jr., J. Appl. Meteorol., 12, 698 (1973).

7. W. Viezee, J. Oblanas, and R. T. H. Collis, AFCRL-TR-73-0708, Air Force Cambridge Research Laboratories, Bedford, MA, (1973), [NTIS No. 776 054].

8. R. H. Kohl, J. Appl. Meteorol. 17, 1034 (1978).

9. R. H. Kohl, J. Appl. Meteorol. 18, 712 (1979).

10. R. T. Brown, Jr., J. Appl. Meteorol. 18, 711 (1979).

11. J. A. Curcio and G. L. Knestrick, J. Opt. Soc. Am. 48, 10, 686 (1958).

12. R. W. Fenn, Appl. Opt. 5, 293 (1966).

13. O. D. Barteneva, Bull. Acad. Sci. USSR No. 12, 1,852 (1960).

14. S. Twomey and H. B. Howell, Appl. Opt. 4, 501, (1965).

15. R. G. Pinnick, S. G. Jennings, P. Chýlek, and C. V. Hamm, to be submitted to J. Atmos. Sciences.

16. H. T. Davis, Introduction to Nonlinear Differential and Integral Equations (Dover, New York, 1962).

17. W. Hitschfeld and J. Bordan, J. Meteorol., 11, 58 (1954).

18. E. W. Barnett and O. Ben-Dov, J. Appl. Meteorol., 6, 500 (1967).

19. P. A. Davis, Appl. Opt., 10, 2099 (1969).

20. F. G. Fernald, B. M. Herman, and J. A. Reagan, J. Appl. Meteorol., 11, 482 (1972).

21. H. Herrmann, Alta Frequenza, 9, 732 (1974).

22. K. N. Liou and R. M. Schotland, J. Atmos. Sci., 28 772 (1971).

23. E. W. Eloranta, Ph. D. Thesis, Dept. of Meteorology, University of Wisconsin (1972).

24. B. M. Golubitskiy, T. M. Zhad'ko, and M. V. Tantashev, Izv. Atmos. Oceanic Phys., 8, 1226 (1972).

25. W. G. M. Blättner and C. M. Lampley, Radiation Research Associates Report RRA-47706, Fort Worth, TX (1977).

26. C. F. Gerald, Applied Numerical Analysis, (Addison-Wesley, Reading, Mass., 1978).

27. R. S. Bonner and W. J. Lentz, Atmospheric Sciences Laboratory Report ASL-TR-0042, White Sands Missile Range, NM (1979).
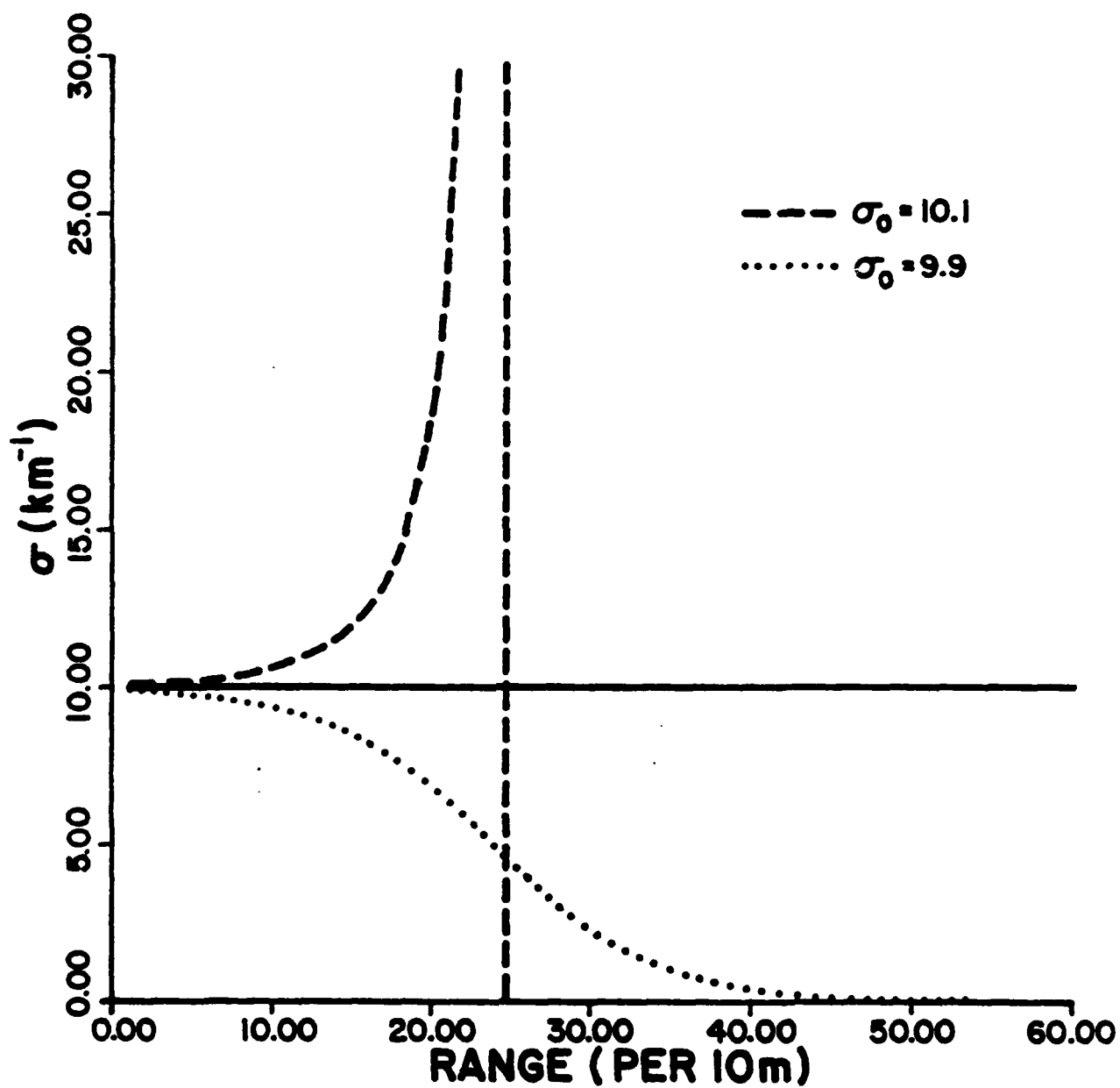
Figure 1 Growth of perturbations in σ due to small errors in the
determination of σ_0.
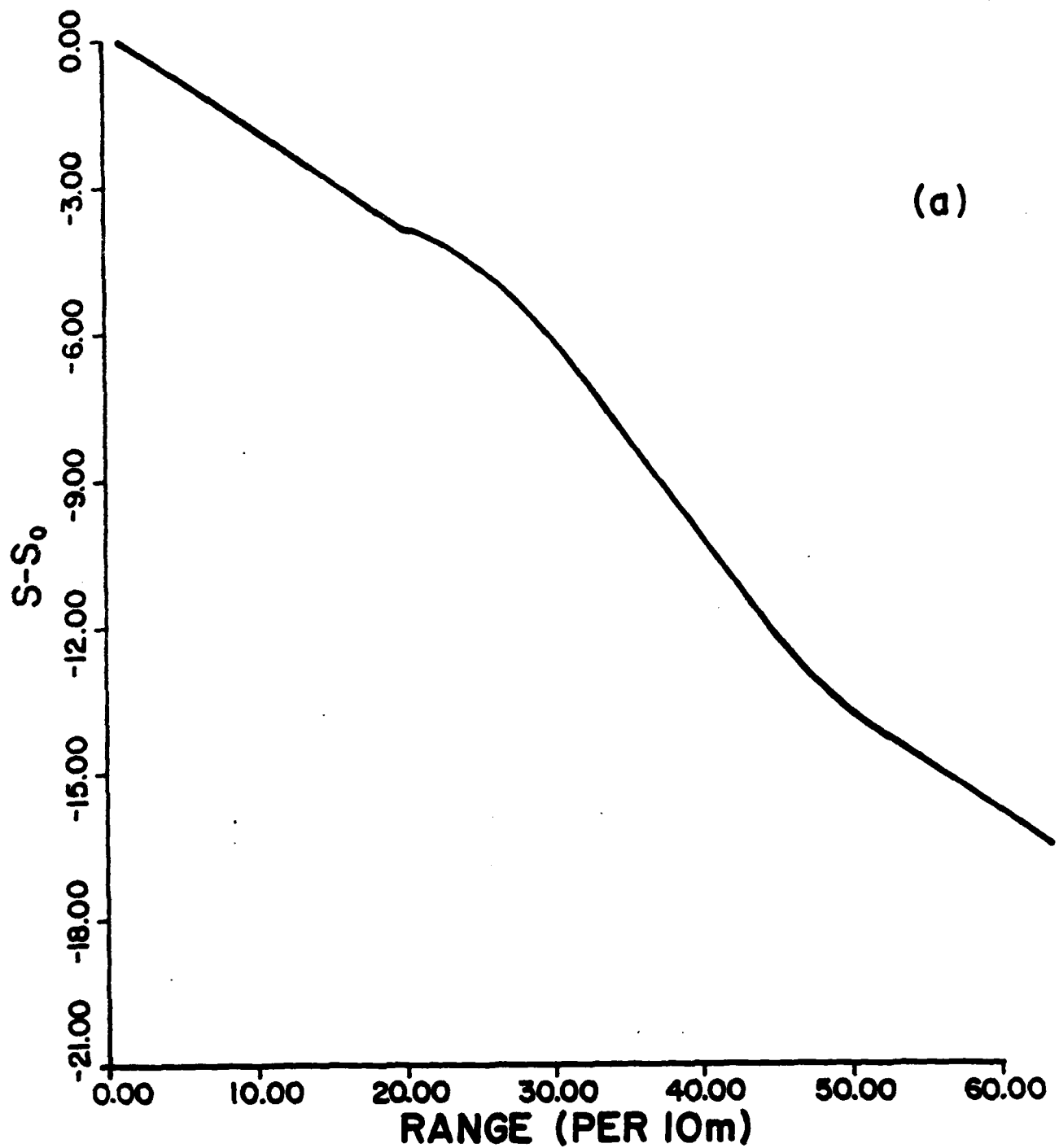
Figure 2 Effect on inversions of errors in the boundary value estimates
of σ.
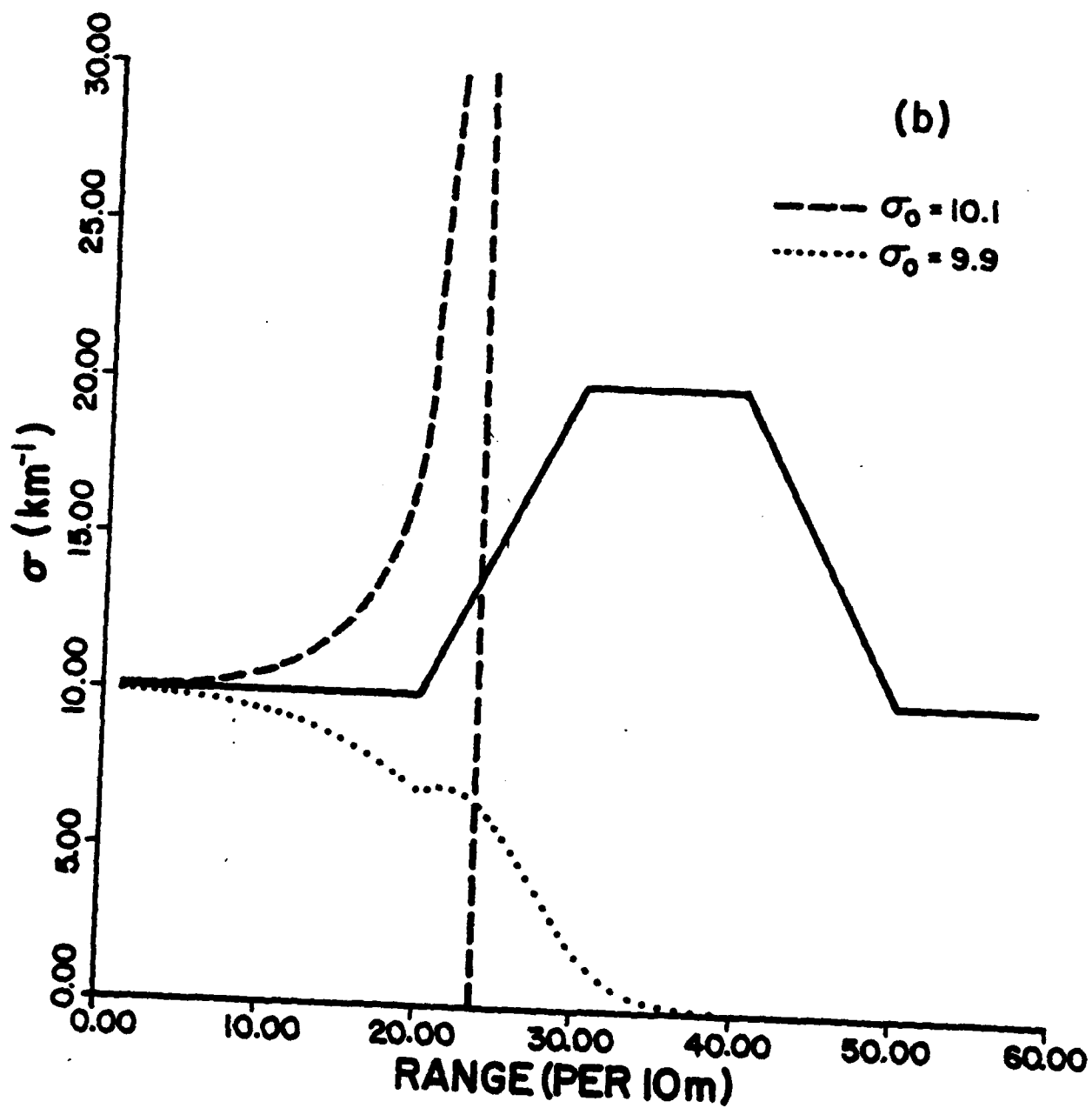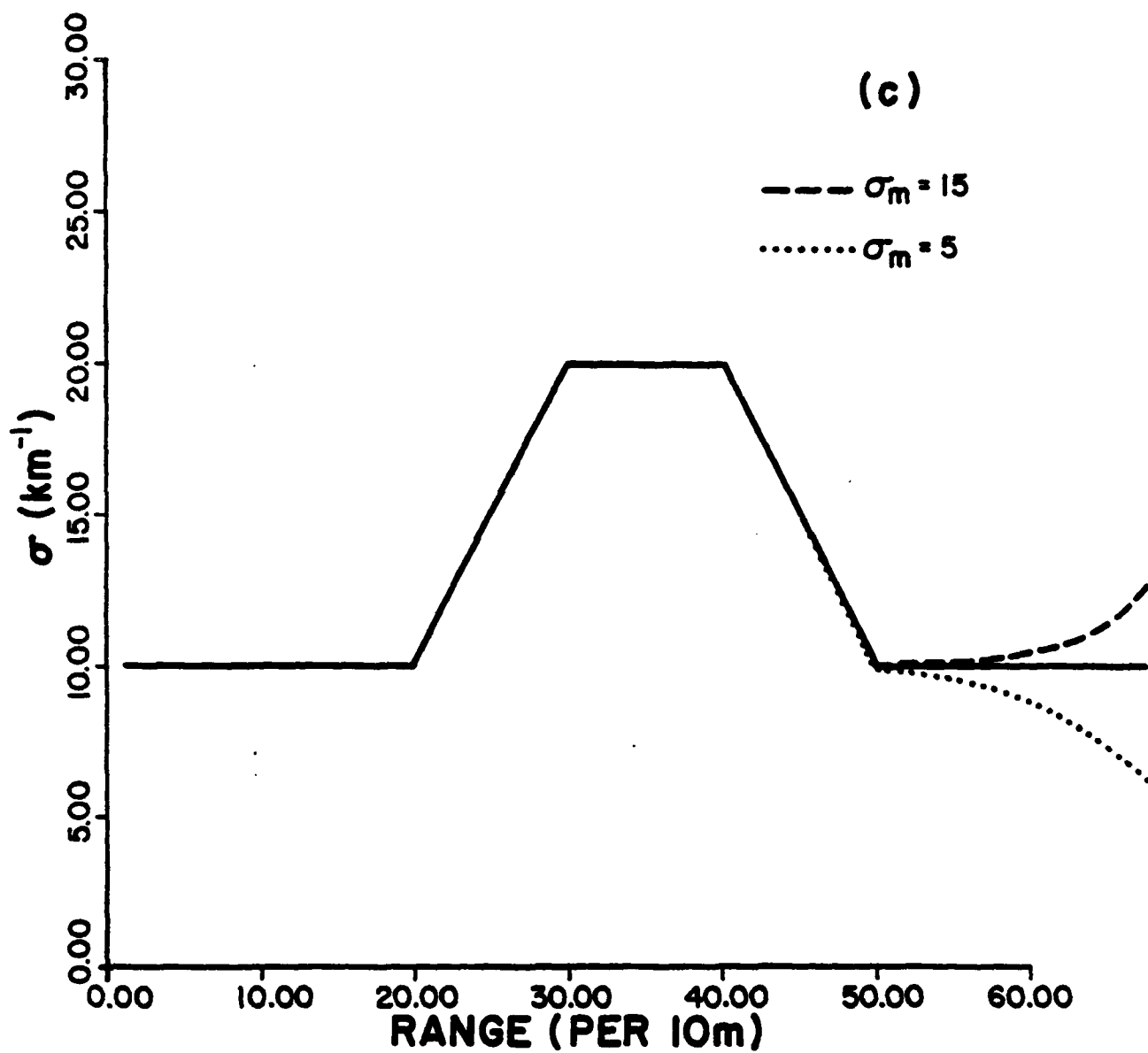
Figure 2. (Cont)

Figure 2. (Cont)
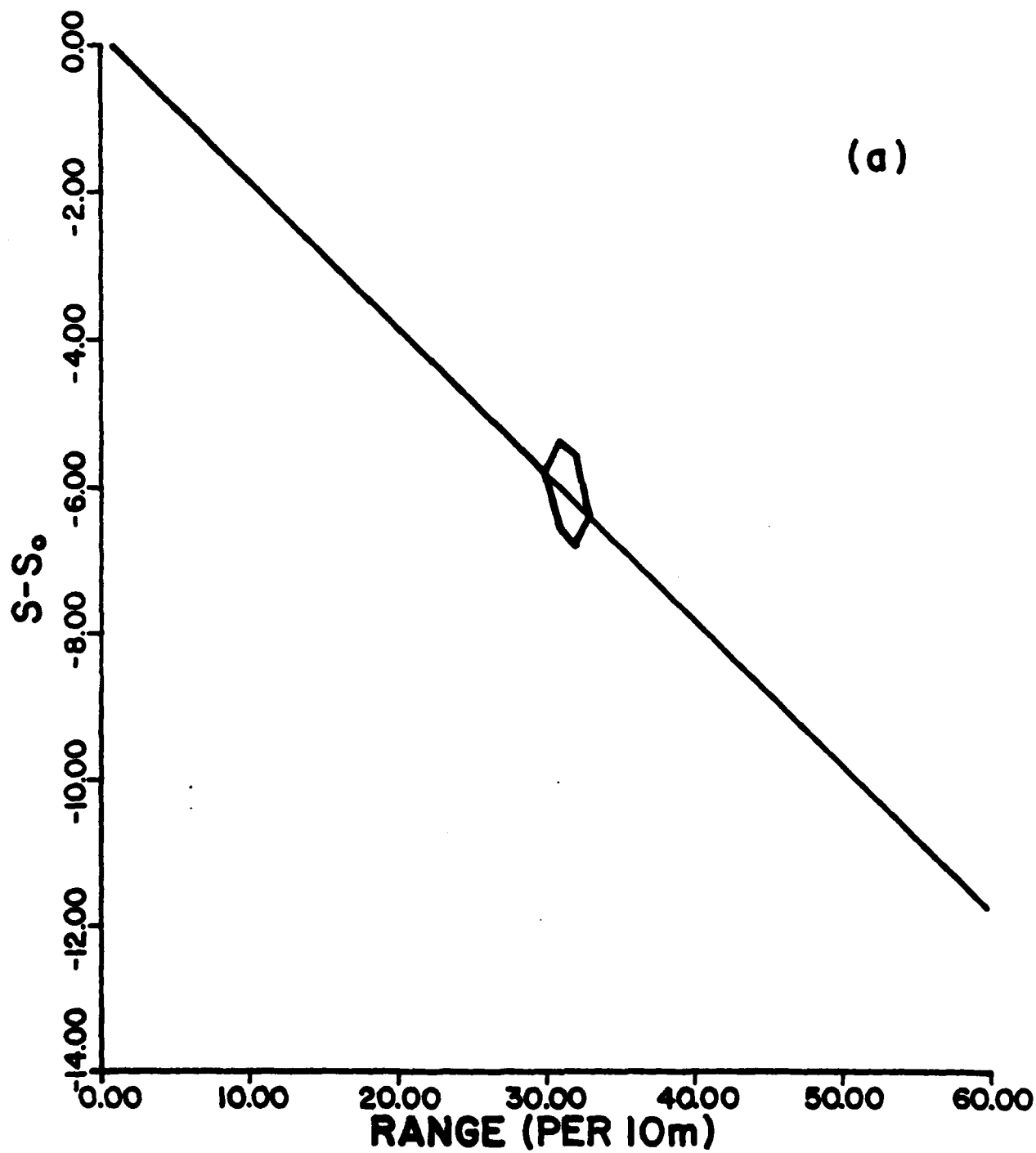
Figure 3 Effect on inversions of simulated signal noise.

Figure 3. (Cont)

32

Figure 3. (Cont)

33
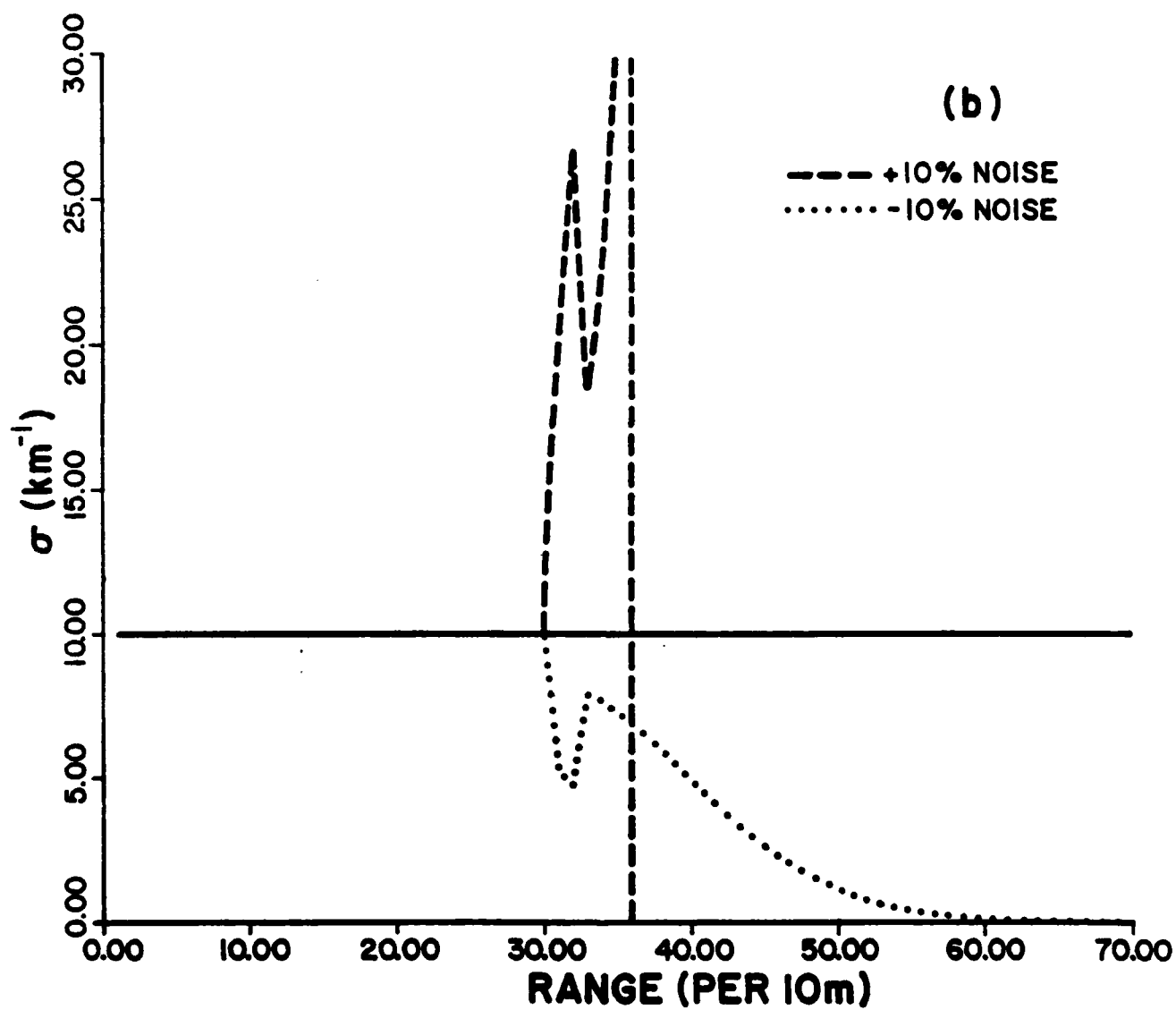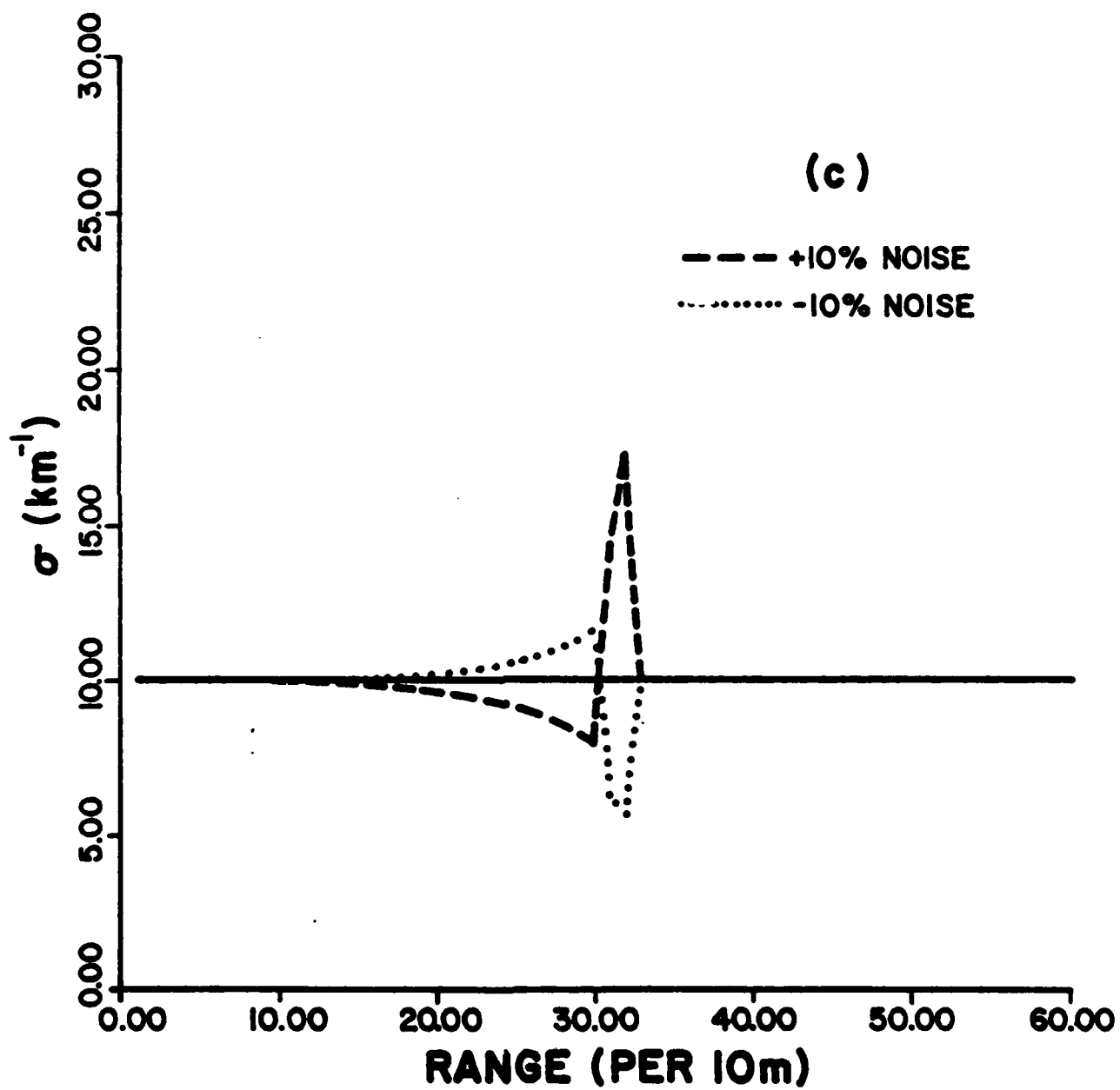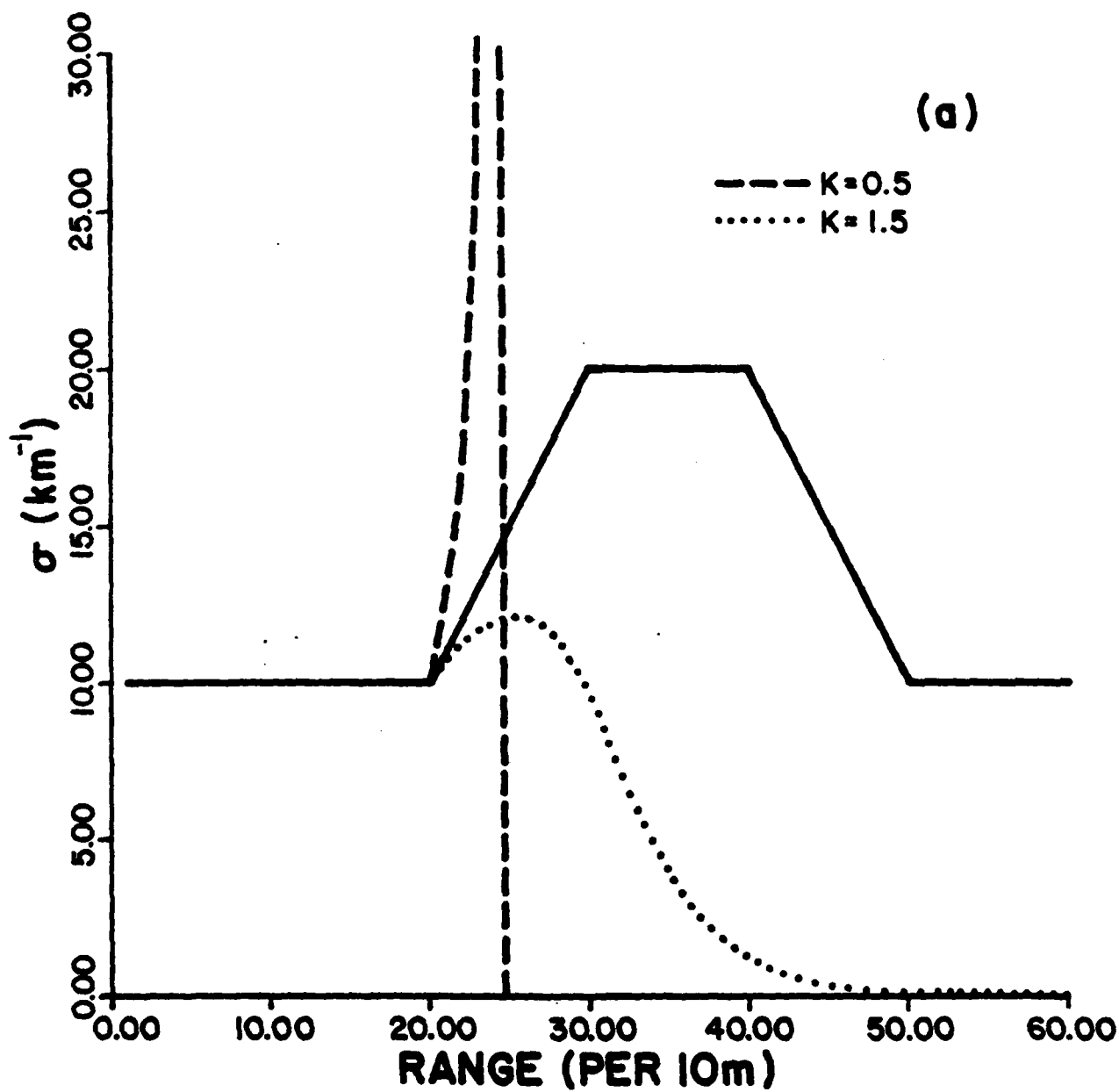
Figure 4   Effect on inversions of value of k.
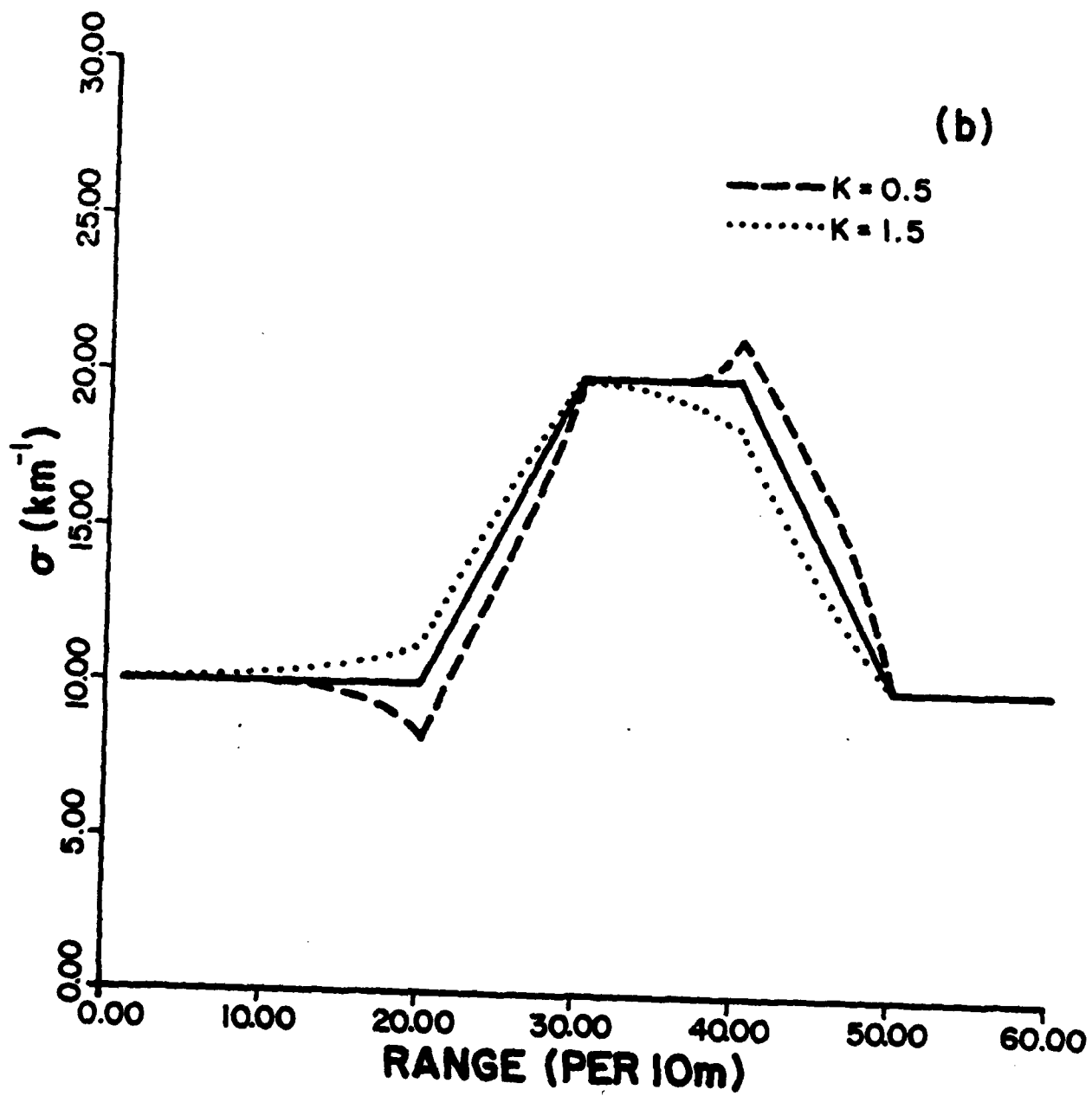
Figure 4. (Cont)
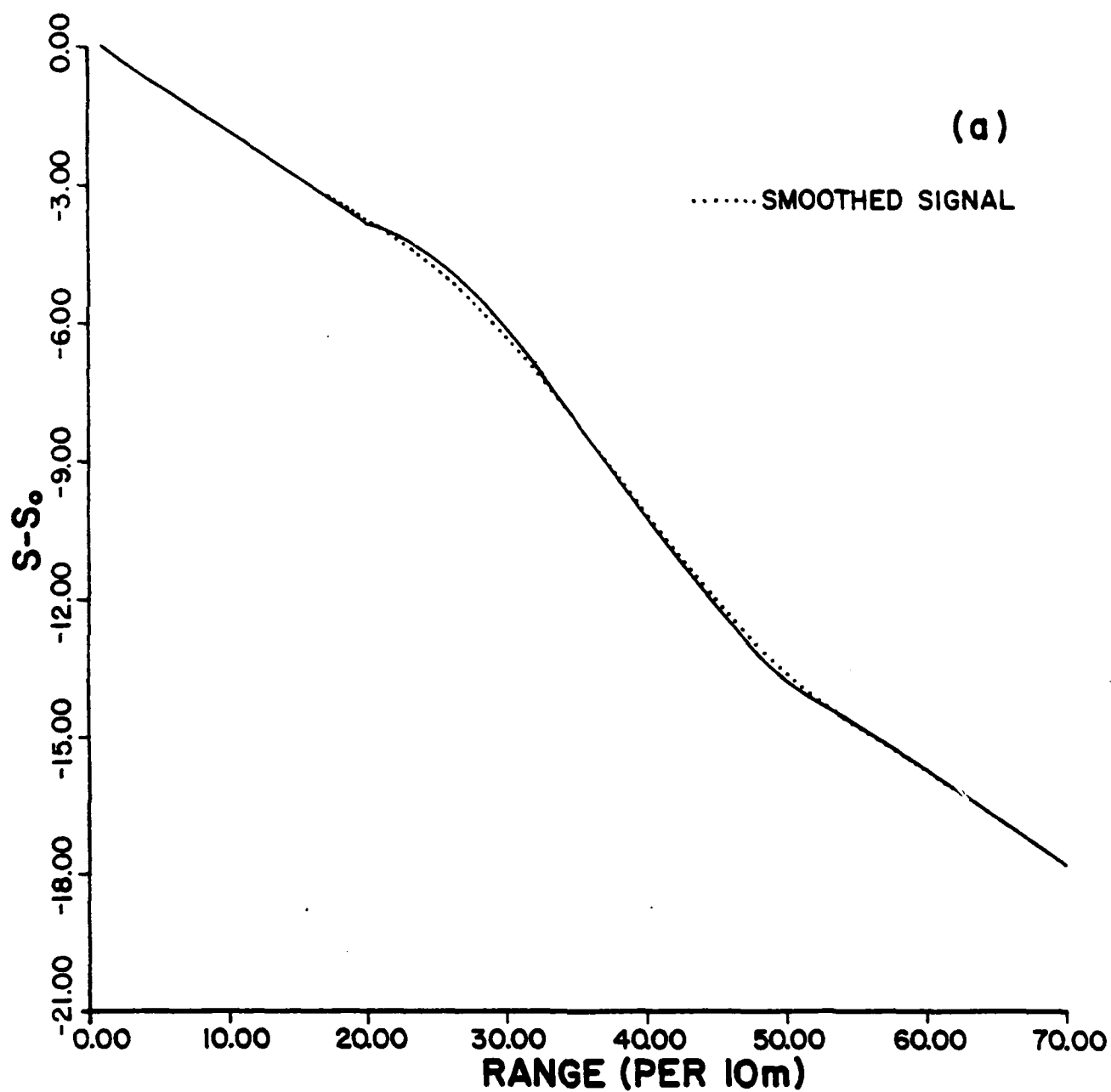
Figure 5   Inversions from Eq. (21), a generalization of the slope method,
for an original and a smoothed signal profile.
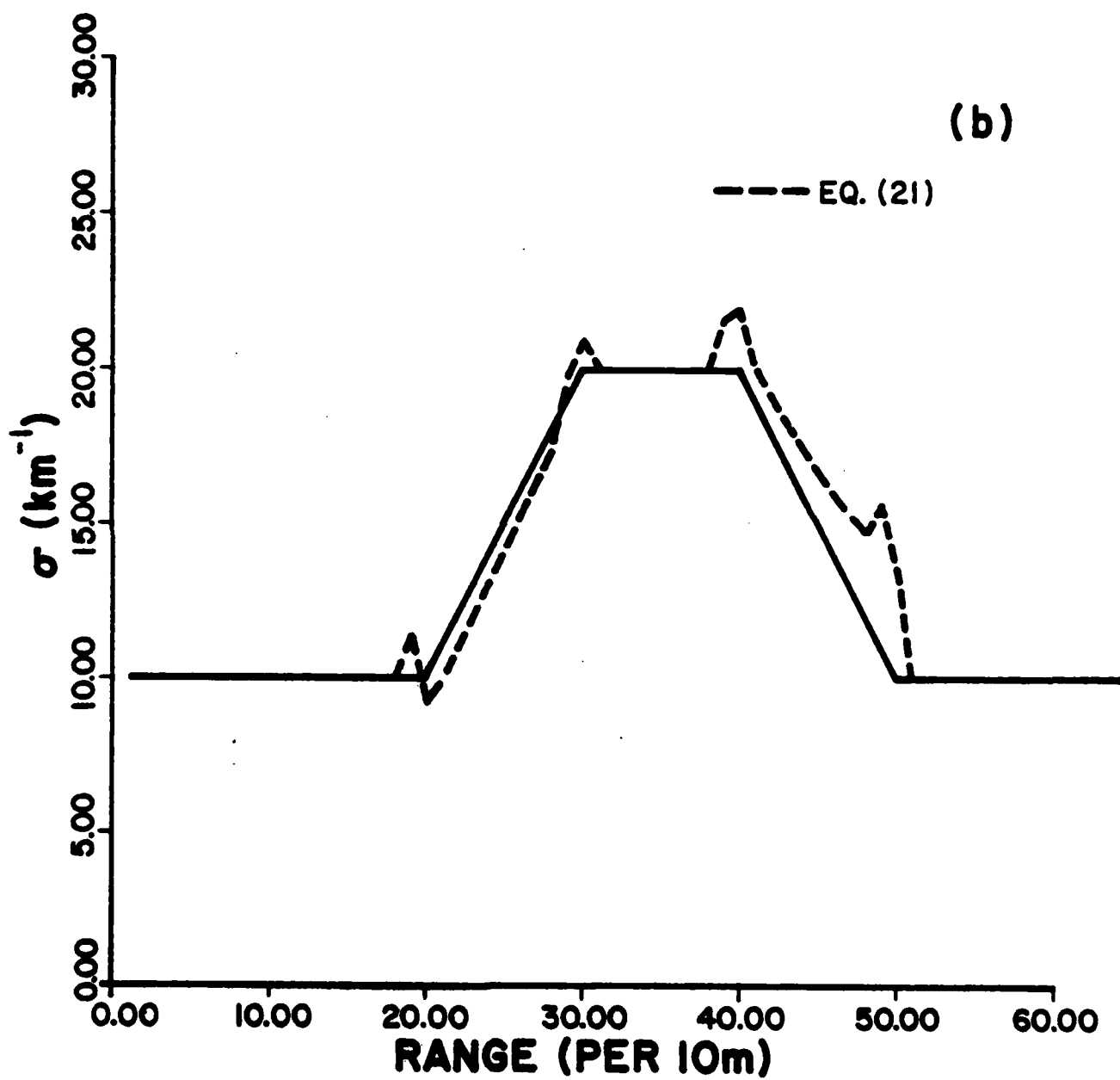
Figure 5. (Cont)
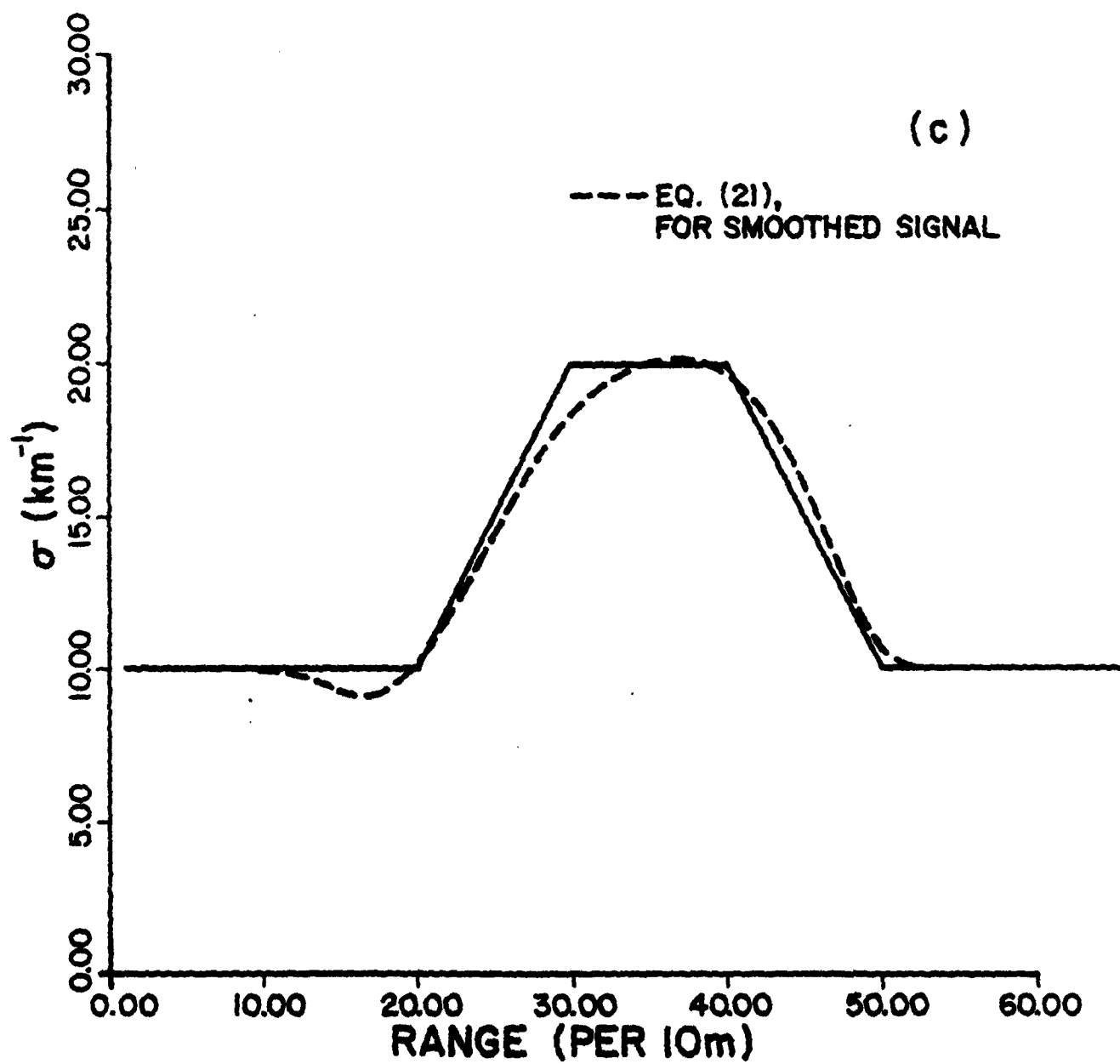
Figure 5. (Cont)
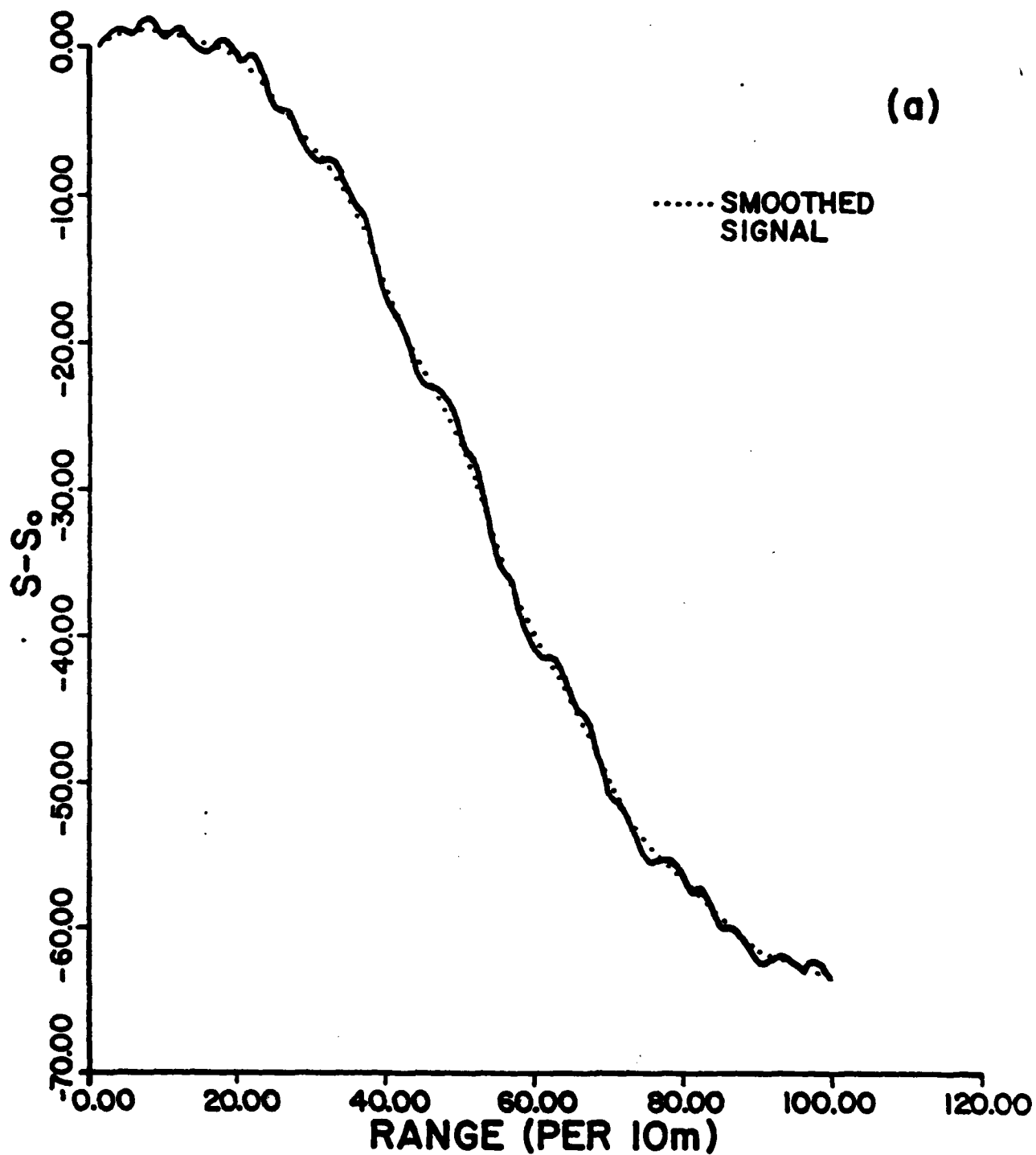
Figure 6   Inversions based on Eqs. (14), (16), and (23) for an unsmoothed
and smoothed signal representing a strongly inhomogeneous
atmosphere.

(b)

····· EQS. (14) & (23) FOR
SMOOTHED SIGNAL

EQS. (14) & (23)

INPUT σ

σ (km⁻¹)

RANGE (PER 10m)

Figure 6. (Cont)

40
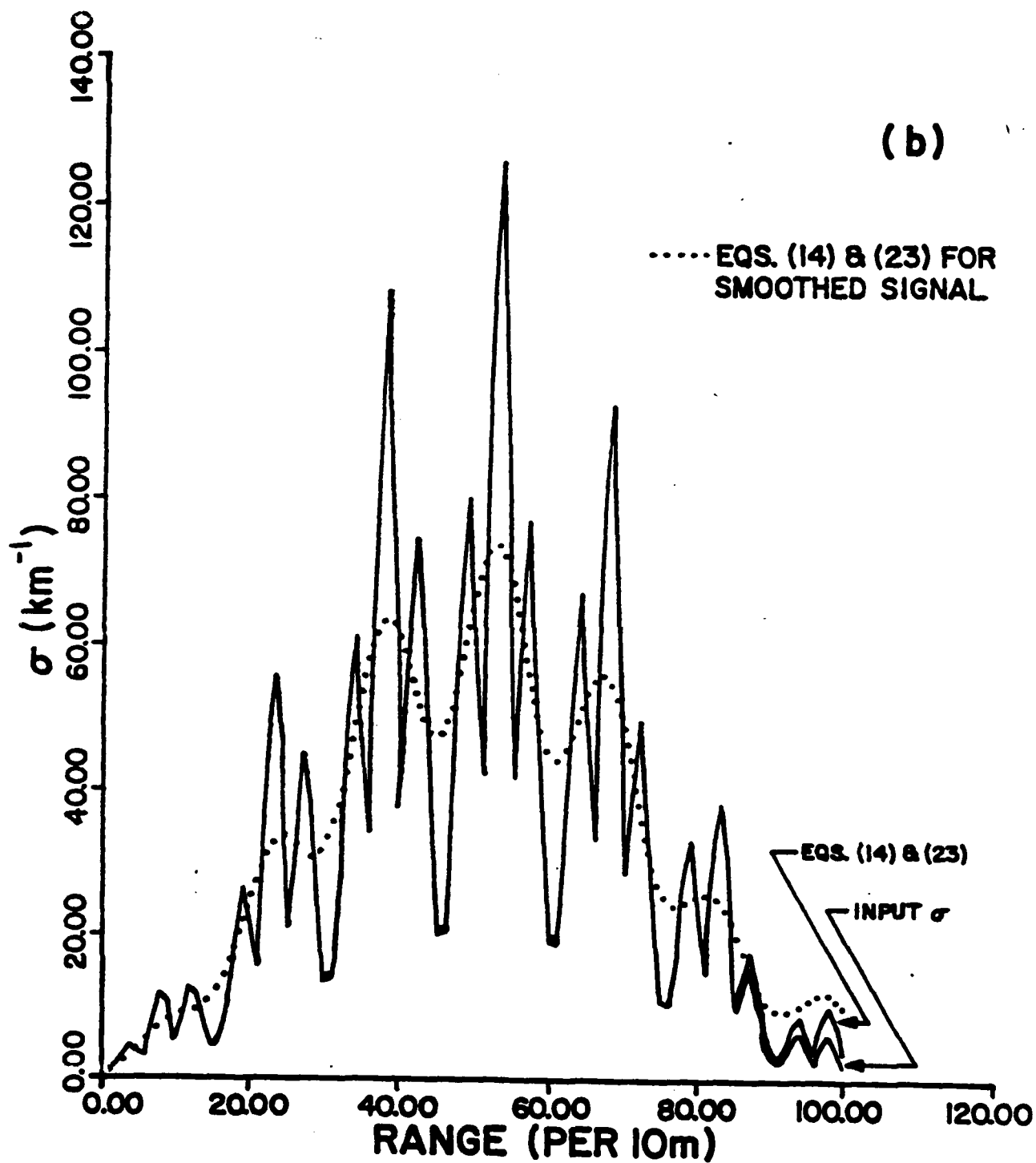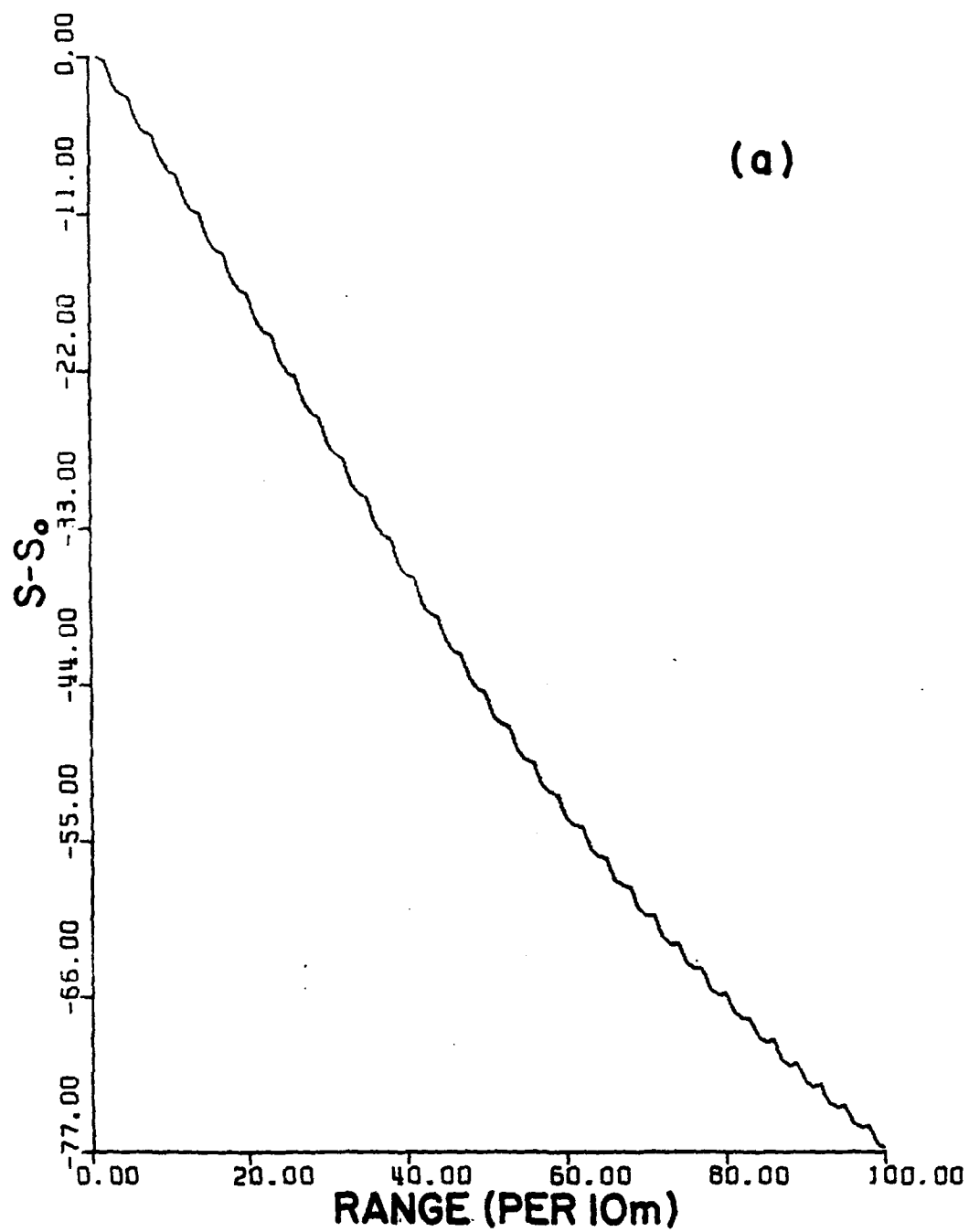
Figure 7 Inversions based on Eqs. (14), (16), and (23) for a very dense, strongly inhomogeneous atmosphere.

Figure 7. (Cont)

42
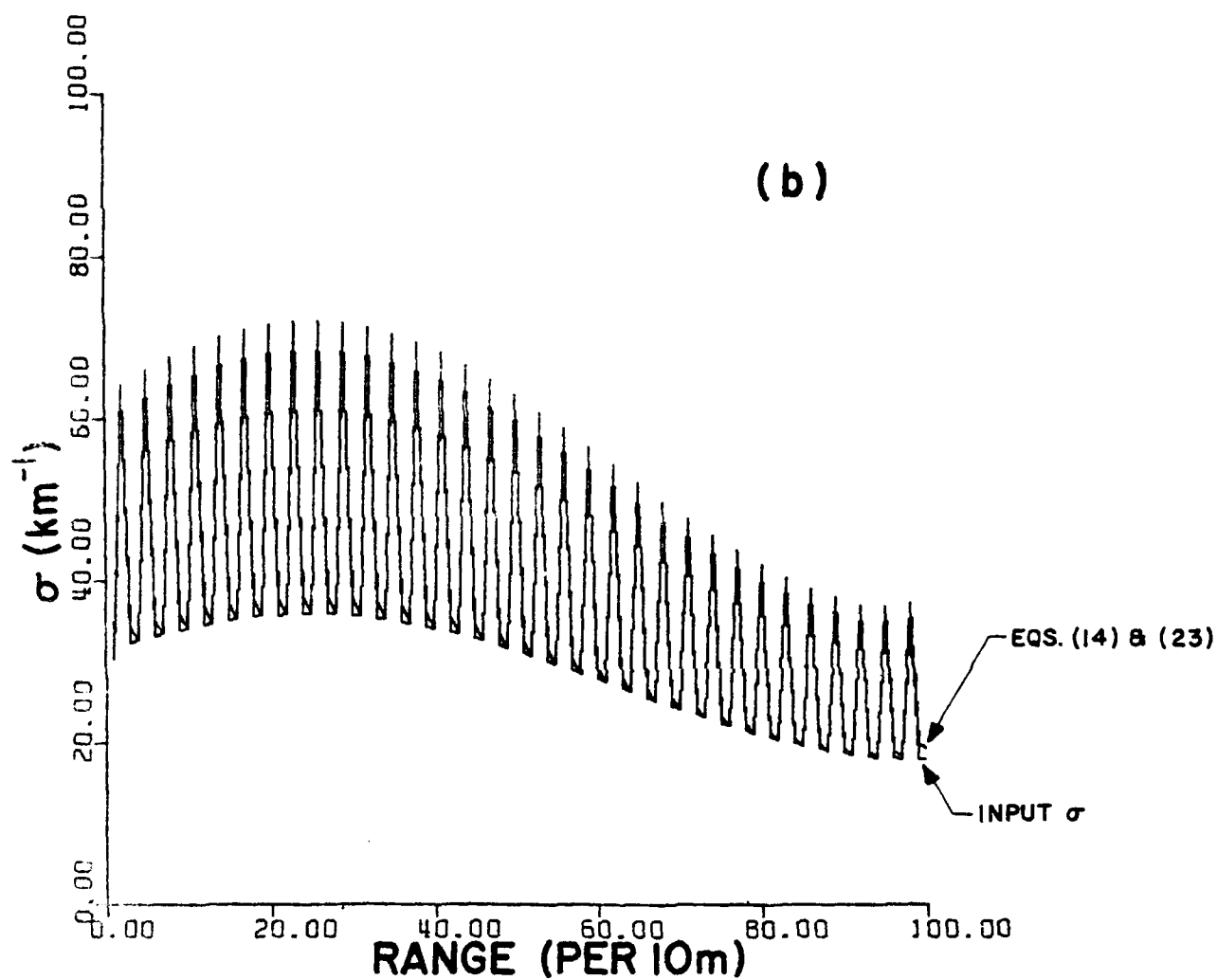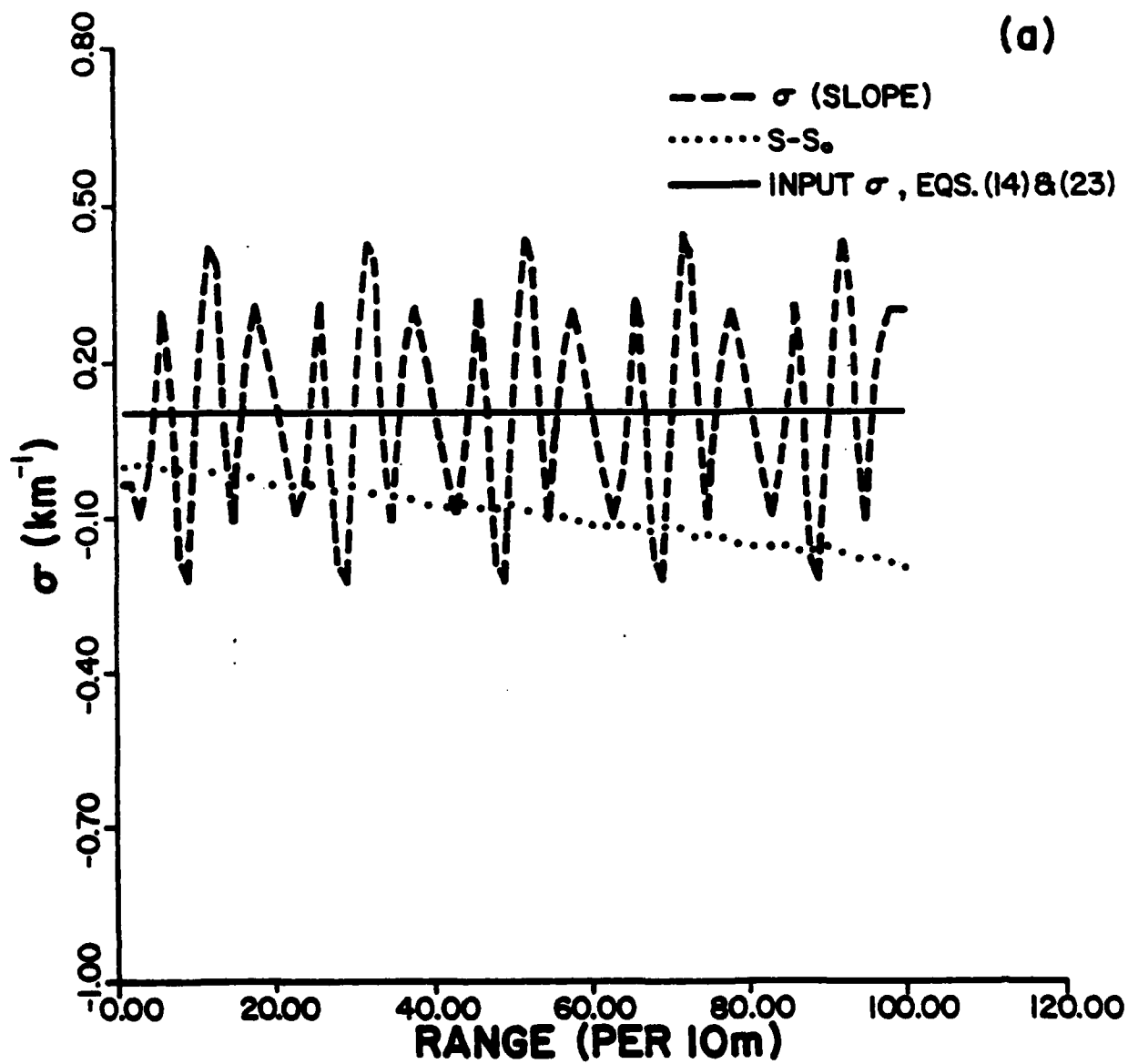
Figure 8 Inversions based on Eqs. (14), (16), and (23), and on the slope method, for a case of high visibility

43

Figure 8. (Cont)

(a)
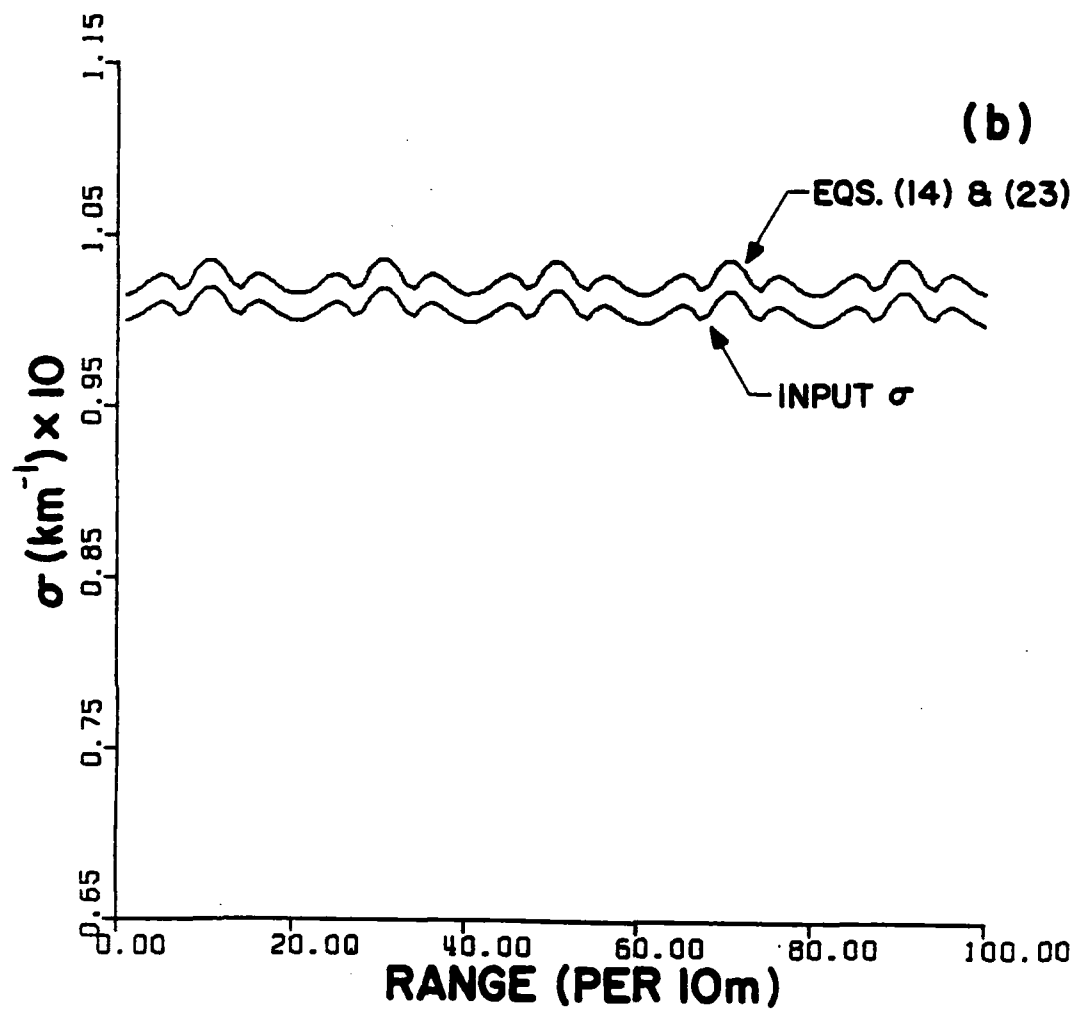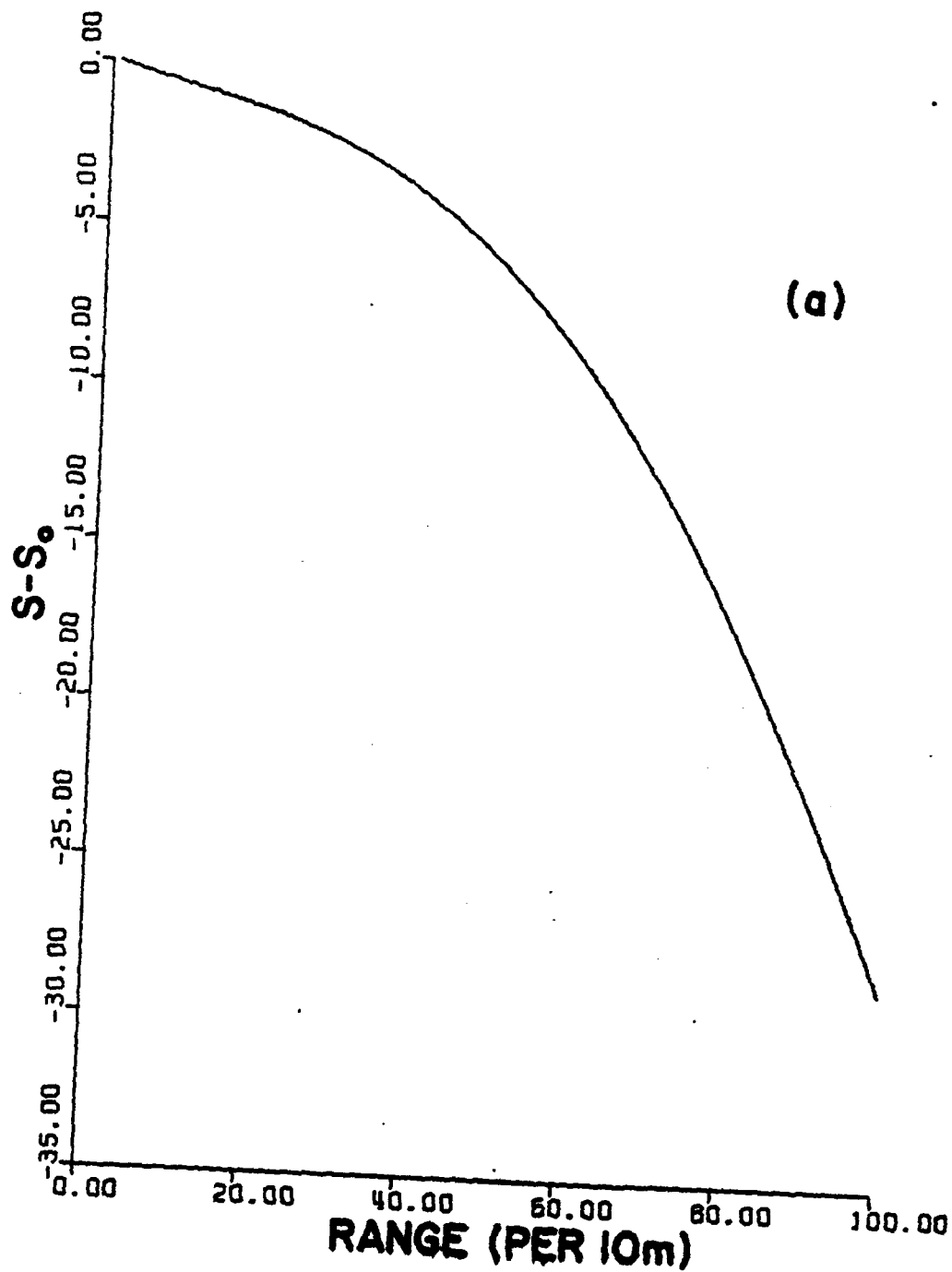
Figure 9   Inversions based on Eqs. (14), (16), and (23), with and without
iteration, for a case of monotonic increasing σ.
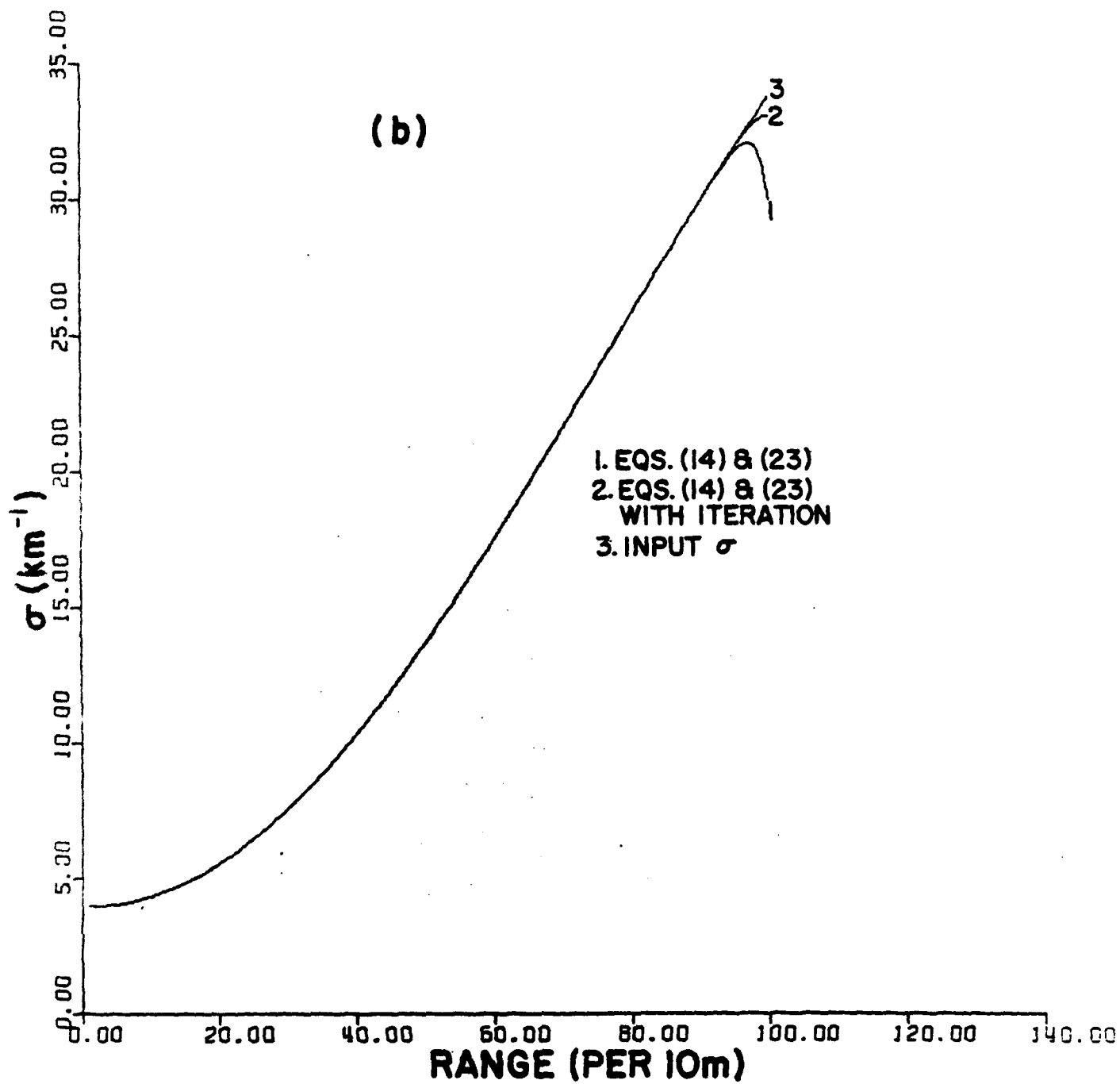
Figure 9. (Cont)
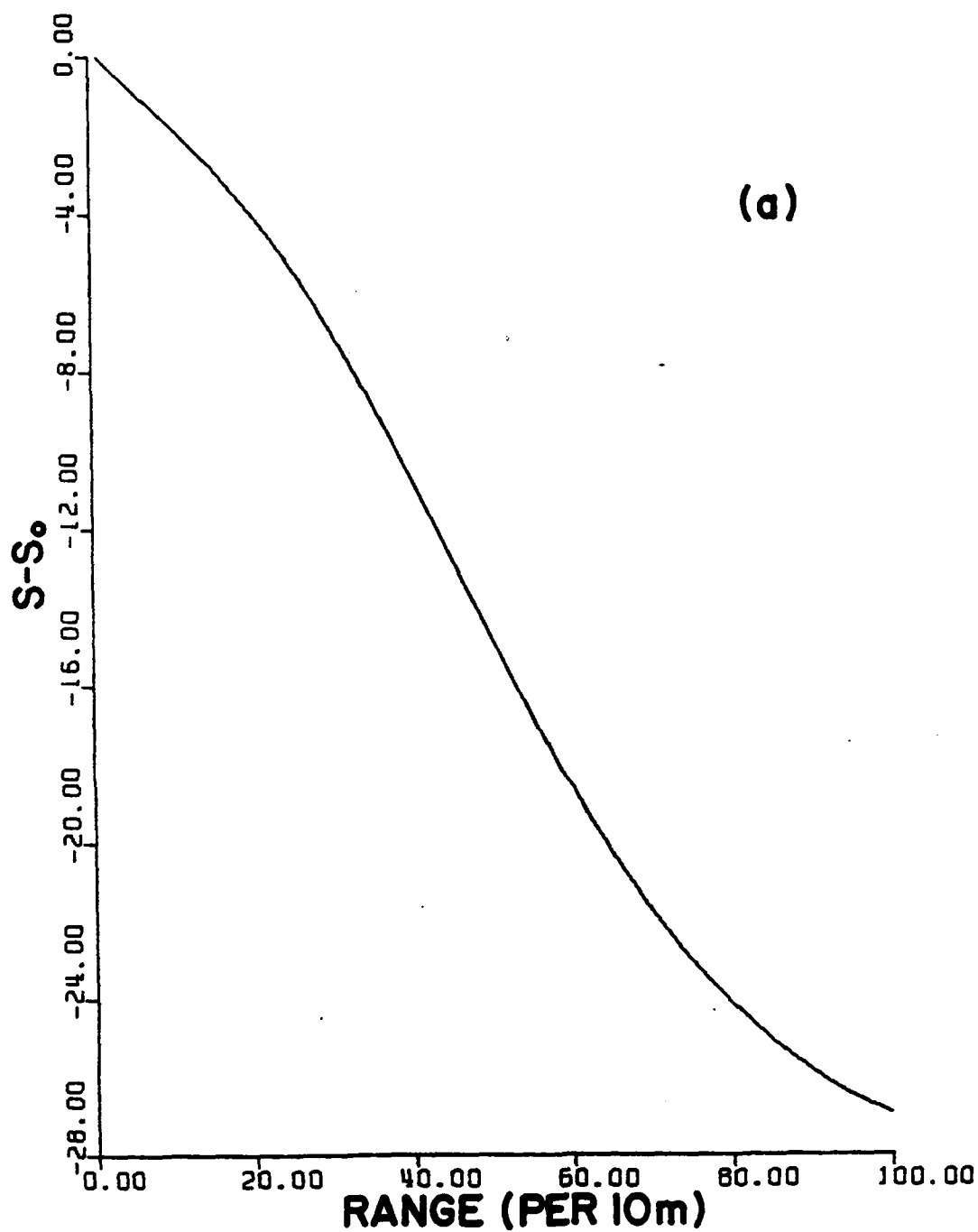
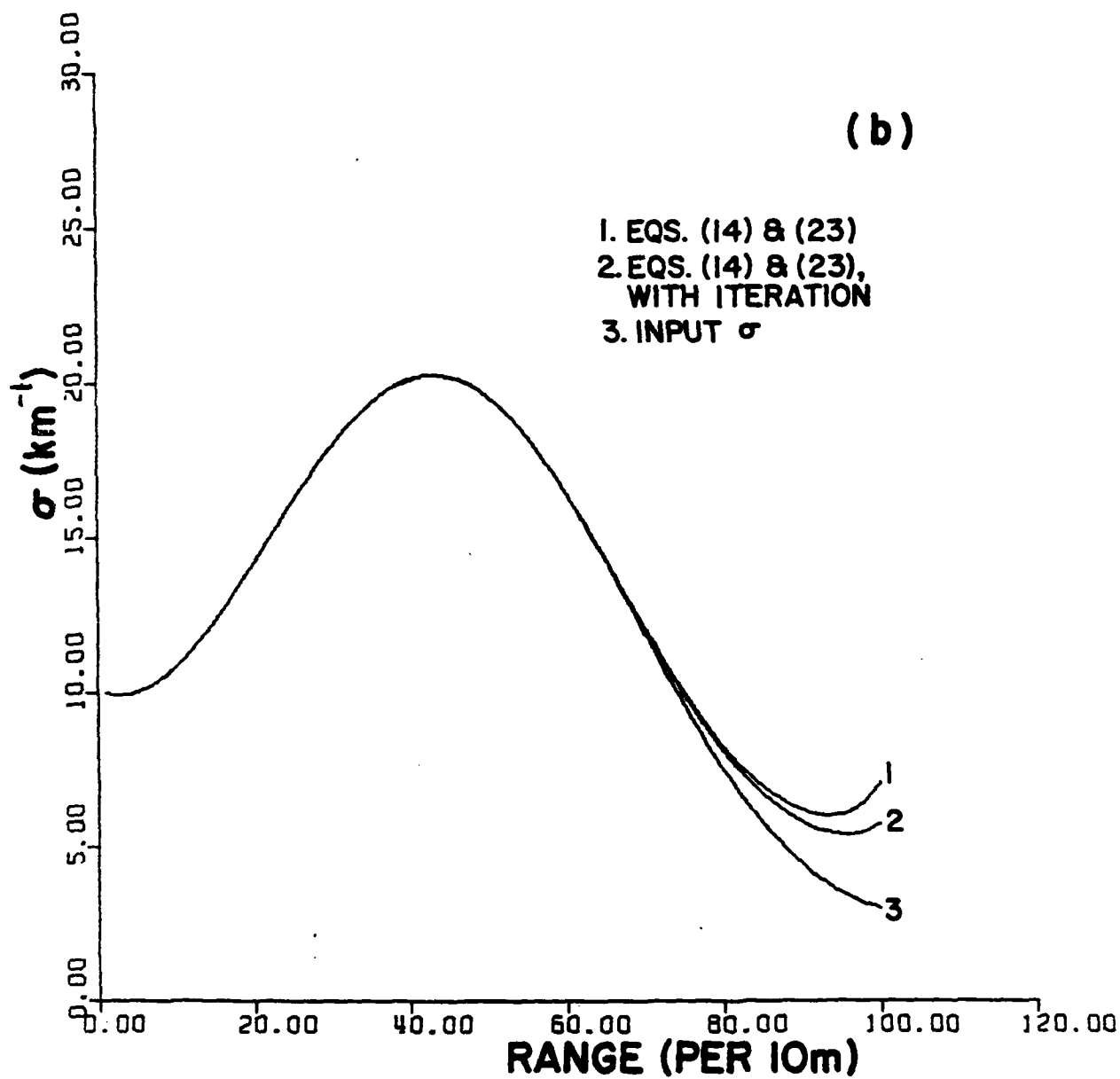Figure 10 Inversions based on Eqs. (14), (16), and (23), with and without iteration, for a case of decreasing σ.
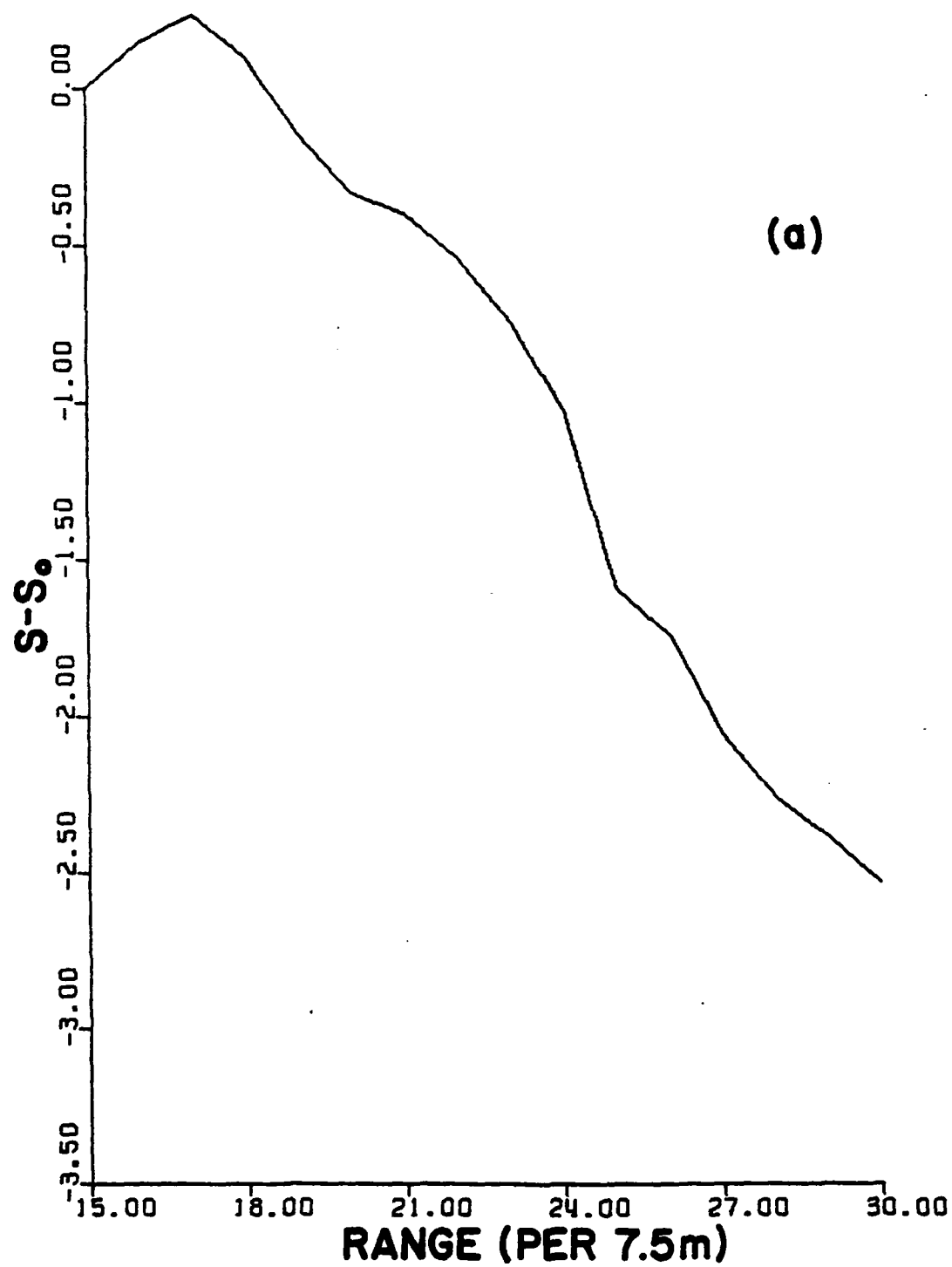
Figure 10. (Cont)

48

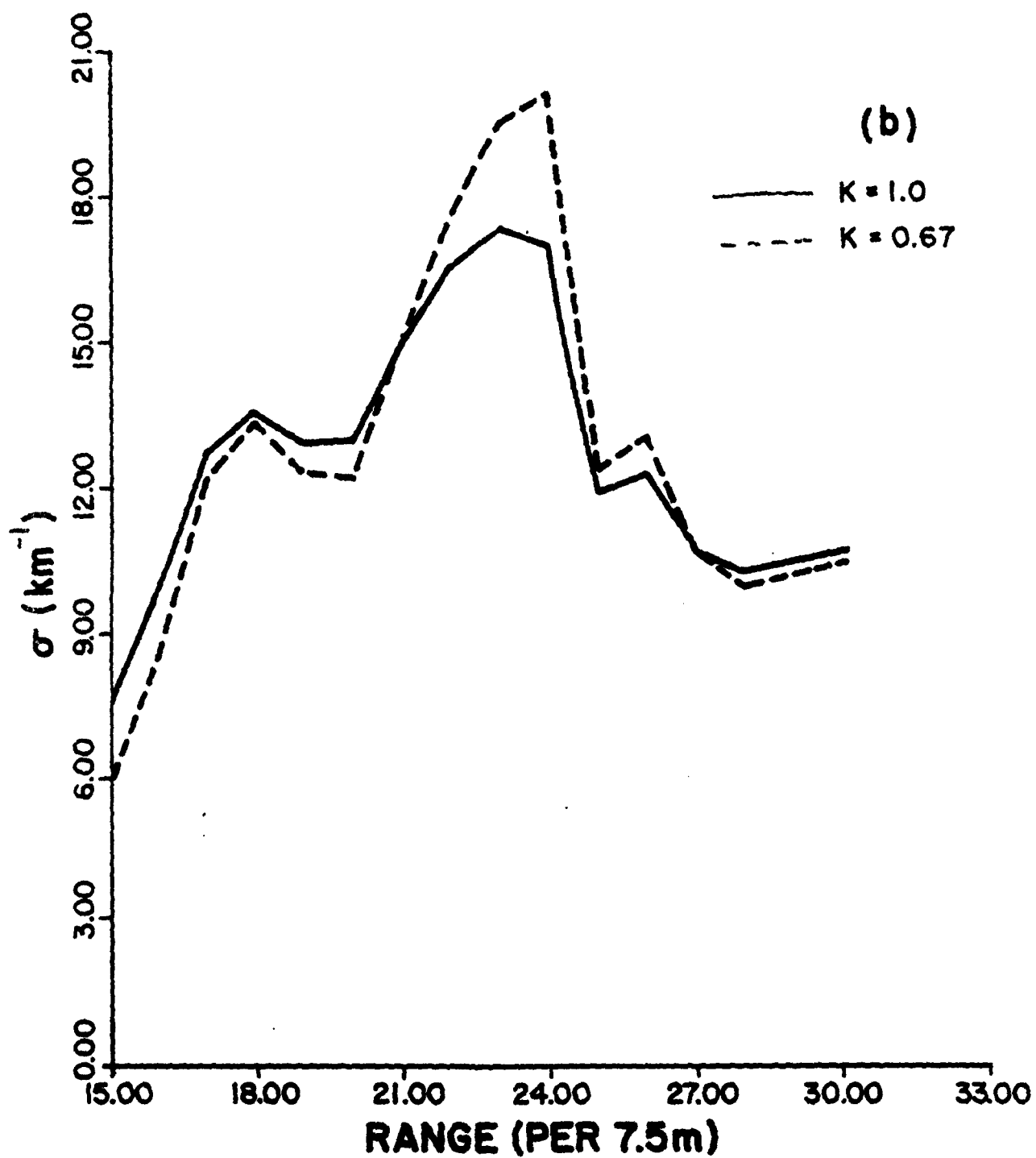Figure 11 Inversions of a real lidar signal, for k = 0.67 and 1.0, based on Eqs. (14), (16), and (23).

Figure 11. (Cont)

ATE
LMED
8